Human iPSC-derived renal organoids engineered to report oxidative stress can predict drug-induced toxicity

Human iPSC-derived renal organoids engineered to report oxidative stress can predict drug-induced toxicity

Lawrence ML[1]+, Elhendawi M[1, 2]+, Morlock M[3], Liu W[4], Liu S[1], Palakkan A[1], Seidl LF[1], Hohenstein P[5, 6], Sjögren AK[7], Davies JA[1]

1. Deanery of Biomedical Sciences, University of Edinburgh, Hugh Robson Building, George Square, Edinburgh, EH8 9XB UK.
2. Clinical Pathology Department, Faculty of Medicine, Mansoura University, Mansoura, Egypt
3. R&D graduate, R&D, AstraZeneca, Gothenburg, Sweden
4. SynthSys Centre for Synthetic and Systems Biology, UK Centre for Mammalian Synthetic Biology, School of Biological Sciences, University of Edinburgh, C.H Waddington Building, Max Born Crescent, Edinburgh, EH9 3BF
5. Leiden University Medical Center, Leiden University, Leiden, The Netherlands
6. The Roslin Institute, The University of Edinburgh, Midlothian, United Kingdom
7 CVRM Safety, Clinical Pharmacology and Safety Science, R&D, AstraZeneca, Gothenburg, Sweden

+ These authors contributed equally to this work

Key words: renal, organoid, hiPSC, kidney, nephrotoxicity, oxidative stress, transporters, oxidative stress reporter, pluripotent, toxicology

Summary

Advances in regenerative medicine have led to the construction of many types of organoids, which reproduce important aspects of endogenous organs but may be limited or disorganised in nature. While their usefulness for restoring function remains unclear, they have undoubted usefulness in research, diagnostics and toxicology. In toxicology, there is an urgent need for better models for human kidneys. We used human iPS-cell (hiPSC)-derived renal organoids to identify HMOX1 as a useful marker of toxic stress via the oxidative stress pathway, then constructed an HMOX1 reporter in hiPSCs. We used two forms of hiPSC-derived HMOX1-reporter renal organoids to probe their ability to detect nephrotoxicants in a panel of blind-coded compounds. Our results highlight the potential usefulness, and some limitations, of HMOX1-reporter renal organoids as screening tools. The results may guide development of similar stress-reporting organoid assays for other stem-cell derived organs and tissues.

Introduction

Nephrotoxicity is a challenging problem in translating drug development to clinical use. A significant proportion of acute and chronic kidney disease is caused by therapeutics in current clinical use. Off-target effects of prescribed drugs cause 19-25% of kidney injury in critically ill hospital patients (Mehta *et al.*, 2004; Uchino *et al.*, 2005). A study at the turn of this century found 1% of all hospital patients over the age of 60 to have suffered drug-induced renal injury (Kohli *et al.*, 2000). The nephrotoxicity of many common drugs arises from the inherent vulnerability of kidney compartments (especially proximal tubules) to toxic insult, caused mainly by the transport systems of these cells concentrating drugs in their cytoplasm. The poor predictive power of animal tests used during drug development, coupled with a lack of established *in vitro*, human-based screens, contributes to difficulties in identifying drug toxicity. Meta-analyses have suggested that correct predictions are made only 50% of the time using animal studies (Fletcher, 1978; Knight, 2008; Hartung, 2009; Archibald, Coleman and Foster, 2011). Poor prediction by animal experiments, in part due to inter-species differences in renal transporter expression (Chu, Bleasby and Evers, 2013; Zou *et al.*, 2018), results in withdrawal of many drugs after their expensive development. It may also explain the high nephrotoxicity of many licensed medicines.

Human cell cultures provide useful test-beds but they have limitations. Primary cultures from human kidneys (for example, biopsies, or organs harvested for transplant but not used) are useful but suffer from problems of reliable supply (Li *et al.*, 2003; Jenkinson *et al.*, 2012; Baverel *et al.*, 2013; Jang *et al.*, 2013; Weber *et al.*, 2016). Recently, developments in stem cell technology have suggested an alternative approach of testing candidate compounds on renal tissue made from human stem cells. Several laboratories have developed methods to differentiate mouse ES cells and human induced pluripotent cells (hiPSCs) to renal lineages and renal organoids (Takasato *et al.*, 2015) (Morizane *et al.*, 2015) (Kim and Dressler, 2005). Testing the response of these organoids to nephrotoxicants has

provided pilot data suggesting renal organoids have potential as an assay system (Xinaris, Brizi and Remuzzi, 2015; Huch *et al.*, 2017; Davies and Lawrence, 2018). Organoids are multicellular entities with many cell types and realistic micro-anatomy, and may therefore be more physiologically relevant than simple 2D monocultures. Their main disadvantages are variability between organoids and a labour-intensive production process, though recent efforts have been made to make small organoids in a semi-automated way (Przepiorski *et al.*, 2018). From the point of view of toxicity testing, the anatomical complexity of organoids can be a drawback, because it makes obtaining a simple quantitative response to toxic stimuli challenging.

In this report, we address the latter problem by designing and constructing a fluorescent reporter system in hiPSCs that reports nephrotoxicity. We first used an established protocol (Takasato *et al.*, 2015) to produce hiPSC-derived human renal organoids and exploited them to identify genes induced by a known test toxicant using RNA-seq. Of the genes identified, *HMOX1* (also known as *HO-1*, a key component of the oxidative stress response) seemed the most promising reporter of stress, and we therefore constructed a fluorescent reporter system to monitor activity of this promoter in hiPSCs. Oxidative stress (OS) can be a direct cause of nephrotoxicity or a secondary effect of toxicity. Thus, this reporter is designed to identify a broad and prominent class of nephrotoxicant, in which the OS response is activated, though it cannot be said to be exhaustive for identification of renal toxicity. Renal organoids were constructed from these genetically modified hiPSCs and their ability to detect nephrotoxicants correctly in a blind-coded panel of compounds was tested.

Results

Transporter expression in renal organoids and identification of HMOX1 as a potential reporter of toxic insult

Renal organoids can be broadly cultured in two ways; as flat organoids, or as truly 3D organoids. Well-established protocols for doing this were used to produce our organoids (Figure S1) (Takasato *et al.*, 2015, 2016). The flat renal organoids were differentiated from hiPSCs and grown in wells and, once differentiated, expressed WT1 (a marker of metanephric mesenchyme and podocytes (Armstrong *et al.*, 1993; Kreidberg *et al.*, 1993)) and CDH1 (an epithelial marker of ureteric bud and distal convoluted tubules (Lee *et al.*, 2013)). They also expressed the glomerular podocyte marker, NPHS1 and the nephron tubule marker, JAG1. The organoids also bound the nephron tubule stain Lotus tetragonolobus lectin (LTL) (Hennigar, Schulte and Spicer, 1985; Barresi, Tuccari and Arena, 1988)) (Figure 1A). 3D renal organoids were made from a modified version of the flat organoid protocol by dissociating and pelleting flat organoids after 7 days of differentiation (Figure S1E). The 3D organoids expressed the podocyte marker NPHS1 and bound the tubule marker LTL. In addition, strongly WT1-positive structures indicated the presence of podocytes, and there was some evidence of CALB-positive structures indicating presence of ureteric-bud like tissue; this was supported by the co-expression of GATA3 and CALB in ureteric-bud tips (Figure 1B).

We tested the expression levels of some renal transporters in both the flat and 3D renal organoids. Flat and 3D organoids expressed *Megalin (LRP2)* and *Cubulin (CUBN)* (Figure 1C). Expression of *OCT2 (SLC22A2)* and *OAT1 (SLC22A6)*, basolateral transporters that are important for renal clearance of some xenobiotics, were also assessed by RT-PCR (Figure 1D). These transporters were more strongly expressed in the 3D organoids than the flat organoids. Transport activity for OCT2 and OAT1 in the 3D organoids was confirmed by performing inhibitable uptake assays (Lawrence, Chang and Davies, 2015) (Çetinkaya *et al.*, 2003) using the fluorescent anion 6-CF (Figure 1E) or the fluorescent cation Asp+ (Figure 1F). This demonstrates the presence of functional transporter proteins in the organoids and that the integrity of the tubular epithelia in healthy untreated organoids was not seriously compromised.

Although some transporters were more strongly expressed in the 3D organoids, the presence of *Megalin* and *Cubulin* in the flat organoids, combined with their increased suitability for high-throughput analyses, led us to adopt this form of organoid to identify a potential reporter for toxic insults in renal organoids. hiPSCs were differentiated into flat renal organoids, and their renal identity was verified by confirming expression of common renal markers (as described above and in the Methods section). We treated these flat renal organoids for 24h with the known nephrotoxicant, gentamicin (Regec, Trifillis and Trump, 1986; Regec, Trump and Trifilis, 1989; El Mouedden *et al.*, 2000), at 1 or 4 mg/ml, leaving some as vehicle-only controls (3 separate organoids per condition). Gentamicin was chosen based on the presence of *Megalin* and *Cubulin* in these organoids since they are the main endocytic receptors involved in gentamicin uptake into proximal tubule cells (Schmitz *et al.*, 2002) and would be expected to be necessary for a realistic toxic response. The transcriptomes of renal organoids in these three conditions were compared using RNA-seq analyses.

Expression of *Megalin* and *Cubulin* was confirmed in the RNA-seq data using gene expression data obtained from the three control samples (Figure S2A). Our RNA-seq results (and other studies (Bajaj *et al.*, 2018)) suggested that, while some important transporters were expressed as expected in flat organoids, others were barely present (Figure S2B). In agreement with our preliminary transporter RT-PCR results, *OAT1 (SLC22A6)* was not detected in the three untreated biological replicates tested. *OAT2 (SLC22A7)* and *OAT3 (SLC22A8)* were also not detected. The expression of *OCT2 (SLC22A2)*, the main transporter responsible for cation uptake on the basolateral membrane of proximal tubule cells, was very low in flat organoid samples. On the other hand, *OATP4C1 (SLCO4C1)*, a basolateral organic transporter for anions over 350 kDa, that is expressed at higher levels in developing murine embryonic kidneys than in adult (Mikkaichi *et al.*, 2004) (Lawrence, Chang and Davies, 2015), was expressed more strongly (Figure S2B). *MRP2 (ABCC2)* and *MRP4 (ABCC4)*, which are the major apical transporters that mediate efflux of anions into the urine, were both expressed. *MATE1*

(SLC47A1), OCTN1, OCTN2 (SLC22A4, SLC22A5), and *P-gp (MDR1)*, the main cation transporters at the apical membrane, were also present (Figure S2C). Although there was little expression of *OCT2, MATE1*, an extrusion protein *in vivo*, has been shown to be capable of apical uptake of at least some cations *in vitro* (Tsuda *et al.*, 2007).

A heat-map of the most differentially-expressed genes amongst all three groups (untreated, 1mg/ml or 4 mg/ml) indicated that the profile of the 4mg/ml gentamicin-treated samples was strikingly different from those of the other groups (Figure 2A). There were no genes expressed significantly differently between the control and the 1mg/ml gentamicin-treated samples (applying a false discovery rate (FDR) cut-off of 0.05). In contrast, treatment with 4mg/ml gentamicin caused the expression of 2221 genes to increase and that of 1770 to decrease. Among the transcripts showing increased expression was *KIM-1* (log fold-change: 1.67; FDR-corrected $p = 0.03$), a biomarker commonly associated with renal tubular necrosis (Table S1). Expression of the oxidative stress marker *HMOX1* was also highly increased (log fold-change: 6.55; FDR-corrected $p = 0.00015$). Other transcripts related to apoptosis signaling and modulation were also highly up-regulated including *LTA, JUN, FOS,* and *HRK*.

To further analyse the transcripts that had increased in the 4mg/ml gentamicin-treated group compared to the control group, we used the 100 most-significantly increased transcripts to perform a gene ontology (GO-term)-enrichment analysis using the PANTHER over-representation test (Mi *et al.*, 2017). The GO terms of the enriched genes included classes highly relevant to toxic insults, including response to toxic substance, detoxification, regulation of cell death, cellular response to stress, response to unfolded and misfolded proteins, chaperone-mediated protein folding and chaperone cofactor-dependent protein refolding (Table S2), implying that the renal organoids had been subjected to stress by the gentamicin exposure.

To find a potential marker that could be used as a reporter for toxicity, we performed a functional classification, using the PANTHER classification

system (Mi *et al.*, 2017). The functional classification was performed using the same 100 most significantly increased transcripts in the high-concentration treated group compared to the control group. The six most-represented gene ontology categories (Figures 2B and 2C) were identified. As functional groupings, these cannot be assigned p-values, but the list of genes can also be analysed using a statistical over-representation test using PANTHER, and these data, together with the p-values, are provided in Table S2. The six ontology categories were further analysed for the intersection of the genes between them to find a marker that could represent the most toxicity response mechanisms. Two genes were found to be common between all six groups: *TRIB3* (2.14 log-fold increase; FDR-corrected $p = 2.15 \times 10^{-5}$) and *HMOX1* (6.55 log fold-change; FDR-corrected $p = 1.4 \times 10^{-4}$) (Figure 2D and Table S5). Since *HMOX1* was found at the center of the functional classifications in our nephrotoxicant-treated renal organoids, and due to the weak evidence for more classical markers of nephrotoxicity, we decided to pursue *HMOX1* as a marker of toxicity in hiPSC-derived renal organoids.

We next treated renal organoids with increasing concentrations of the nephrotoxicant gentamicin, or cisplatin to test the organoid expression of HMOX1 in response to known nephrotoxicant drugs. We also stained drug-treated organoids for HMOX1 together with LTL and COL IV (figure S3A), or JAG1 (figure S3B), to test whether the response is localized to a specific cell type in the organoid. HMOX1 expression increased in response to the toxic drugs but that increase was not limited to a specific renal structure. The general increase in HMOX1 expression in response to the toxic drugs, rather than specific response in proximal tubular cells, the primary site of toxicity of both drugs, could be due to the availability of the drug to all cell types of the organoid through the media in contrast to what happens *in-vivo* where these drugs filter through the glomeruli then specifically accumulate inside the proximal tubular cells, through apical uptake pathways, where most of their toxic effect is seen.

HMOX1 oxidative stress reporter hiPSC cell lines

Having identified *HMOX1* as an important marker of renal toxicity and confirmed its response to gentamicin in our renal organoids, we used CRISPR technology to insert a fluorescent reporter (mCherry) into the *HMOX1* locus to report on its expression. We included a 2A-peptide upstream of the mCherry sequence to uncouple the HMOX1 protein and the reporter protein. (Figure 3A). Clonal lines were established and further experiments were carried out on a homozygously-targeted clone (*HO1*-mCherry-hiPSCs).

To test the response of the *HO1*-mCherry-hiPSCs, still in their undifferentiated state, we treated one of the cloned hiPSC lines with different concentrations of hydrogen peroxide to induce oxidative stress (0, 125 or 250 μM) for 24h. Fluorescence increased in a dose-dependent manner (Figure 3B and C). This increase in fluorescence reflected the increase in *HMOX1* transcripts in response to increasing hydrogen peroxide concentrations, measured by qPCR (Figure 3D). In order to verify that insertion of the reporter downstream of the *HMOX1* locus did not affect the ability of the cells to differentiate into flat renal organoids, we differentiated the *HO1*-mCherry-hiPSC line into flat renal organoids, as we had for the hiPSC parent line. After 18-20 days of differentiation, differentiated cells were stained for the presence of renal markers (GATA3, JAG1, PAX2, CDH1), confirming that the reporter hiPSCs could be differentiated into renal organoids (Figure 3E). To further validate the cellular co-expression of HMOX1 and mCherry, undifferentiated hiPSCs induced with 150μM hydrogen peroxide were co-stained with either HMOX1 and mCherry antibodies (Figure 3F, top panel), or with HMOX1 antibody only and imaged together with mCherry fluorescence (Figure 3F, bottom panel).

Renal organoids derived from the HO1-mCherry-hiPSC oxidative stress reporter cell line predict toxicity from known nephrotoxicants

The overall aim of this work was to generate renal organoids that would report toxic insults by means of an easily read fluorescent signal. To determine

whether the reporter cell line could detect oxidative stress when the cells were differentiated into renal organoids, we treated them with gentamicin and cisplatin. These compounds are known to cause renal toxicity, either through direct induction of oxidative stress or as a secondary response to renal toxicity (Karatas *et al.*, 2004; Miller *et al.*, 2010; Morales *et al.*, 2010). Importantly, these compounds gain entry to the cell through specific renal transporters, unlike the hydrogen peroxide used to induce oxidative stress in the undifferentiated hiPSCs. The concentrations of cisplatin and gentamicin chosen were based on previous *in vitro* renal toxicology studies (Regec, Trump and Trifilis, 1989; Jun *et al.*, 2018) (Bajaj *et al.*, 2018).

Fluorescence intensity increased in a dose-dependent manner in the flat organoids treated with increasing amounts of either cisplatin (Figure 4A, B) or gentamicin (Figure 4D, E), with a similar increase in *HMOX1* gene expression measured by qPCR (Figure 4C, F). The increases in reporter and gene expression are not identical, probably because the half-lives of the mCherry fluorophore and the *HMOX1* transcript are not the same, with the fluorophore able to persist in the cell for longer (Shaner *et al.*, 2004; Snapp, 2009). We also noticed that our cisplatin-treated organoids had a visibly greater loss of structure and tissue integrity than the gentamicin-treated organoids, probably due to the difference in mechanism of toxicity of the two compounds (data not shown).

Response of HO1-mCherry-hiPSC-derived renal organoids to a blind-coded panel of drug compounds

Due to the differential expression of various uptake and efflux transporters assessed by RT-PCR in both flat and 3D organoids, and by RNA-seq transcript analysis in flat organoids, we used both flat and 3D organoids to test the usefulness of the *HO1*-mCherry-hiPSC line for predicting renal toxicity.

A panel of blind-coded compounds was produced, that included known nephrotoxic compounds, non-toxic compounds, and compounds that are not considered toxic to kidneys (but that might still be toxic to other organs). The compounds, selected and supplied by the Gothenburg authors without revealing their identities to the Edinburgh authors, were as follows: the control compound, not expected to be toxic, was dexamethasone. The example of a non-nephrotoxic compound that may be toxic to other organs was ketoprofen, which induces oxidative stress (Cheng *et al.*, 2014) through effects on the mitochondria (van Leeuwen *et al.*, 2012), and has its main toxic effect in the gastrointestinal tract. Examples of nephrotoxicants included puromycin, cisplatin, gentamicin, cidofovir and ifosfamide (Ho *et al.*, 2000; Barnett and Cummings, 2018) (Akilesh *et al.*, 2014).

HO1-mCherry-hiPSC renal organoids (both flat and 3D) were incubated in a four-fold dilution series of each compound for either 24h or 72h. Data on reporter expression is shown graphically in Figure 5. For dexamethasone, while there was some noise in the data, none of the concentrations produced a signal statistically different ($p<0.05$) from other concentrations (including zero), in either the flat or 3D cultures. Thus, the reporter cells correctly identified dexamethasone as non-toxic. The gastrointestinal toxicant ketoprofen induced a significant response in the flat cultures at the two highest concentrations, and in the 3D cultures only at the highest concentration after 72h.

For puromycin, both flat and 3D organoids showed a significant rise in fluorescence after both 24 and 72h, with a stronger response after 72h. Cisplatin induced a significant increase in fluorescence, both in flat and 3D organoids. Again, the 3D organoids responded to lower concentrations than the flat ones, and changes were more evident after 72h than after 24h. For gentamicin (which was the toxicant we used to identify *HMOX1* as a potential reporter), the 24h-treated organoids of both flat and 3D types responded to even low concentrations (6μM for 3D organoids, 24μM for flat organoids). For this compound, the 24h time point was more informative than 72h. Ifosfamide

induced a significant fluorescence increase in both flat and 3D organoids, at both 24h and 72h. After 24h, 3D organoids were more sensitive than flat organoids but, at 72h, the flat organoids were more sensitive predictors of toxicity. Organoids did not predict cidofovir toxicity as reliably as for the other compounds. Flat cultures treated for 24h showed no significant response, while treatment for 72 hours elicited a response at even the lowest concentration tested. The 3D cultures, however, showed a response after 24h treatment but not after 72h.

Taking successful prediction of a toxin to be response at $p<0.01$, and successful prediction of non-toxic nature to be absence of a response even at $p<0.05$, the success of the *HO1*-mCherry-hiPSC-derived organoids at predicting toxicity is summarized in Figure 6. As can be seen from Figure 6, no single combination of timing or organoid shape was completely reliable at prediction. Using a combination of 24h and 72h and taking a Boolean OR of the results (where any positive data point is considered to mean an overall 'positive'), the organoids correctly predicted toxicity for all nephrotoxic compounds. The 3D organoids also did not predict toxicity for either the non-toxic dexamethasone or the GI oxidative stress-inducer ketoprofen, unlike the flat organoids that did predict toxicity for ketoprofen at the highest concentrations.

Discussion

The purpose of this study was primarily to find a reporter of toxicity that could be engineered into human pluripotent stem cells, and then to assess the performance of that reporter using a blind-coded panel of test compounds. In our RNA-seq analyses, classical markers of nephrotoxicity were either not up-regulated in response to injury (*CLU*) or were down-regulated (*NGAL*) (data not shown) in response to the known nephrotoxicant gentamicin. Although *KIM1*, a classical *in vivo* renal injury marker, was weakly up-regulated in the RNA-seq analysis, reports on its suitability for *in vitro* nephrotoxicity screening in cell culture models are variable. (Adler *et al.*, 2016) (Li *et al.*, 2013) (Huang *et al.*, 2015). Conversely, Alder et al. also found that *HMOX1* was a much

more sensitive marker for predicting nephrotoxicity in 2D and 3D microfluidic HPTEC cells. The renal organoids most closely resemble human embryonic kidney tissue as shown by the authors of the protocol (Takasato *et al.*, 2015, 2016), providing an explanation for the lack of induction of classical injury markers such as Kim-1 following injury. An advantage of targeting immediate responses to stress is that even immature tissues will respond. Based on the intersection of *HMOX1* in several different toxicity pathways as well as its greater level of up-regulation, we identified *HMOX1* as a potentially promising reporter for one large class of nephrotoxicants; those in which the OS pathway is activated. We engineered the gene for the fluorescent protein mCherry into the locus of *HMOX1* in hiPSCs and showed that organoids made from those hiPSCs can predict toxicity, at least when used with a range of concentrations and measurements done at more than one time point. It is important to note that our assay, using renal organoids alone, does not discriminate between a toxicant dangerous only to kidneys, and one dangerous to other tissues as well.

In our trial of the *HO1*-mCherry-hiPSC-derived organoids, there was a trend for 3D organoids to be more sensitive than flat ones (that is, to respond to lower concentrations of test compounds). This difference was especially marked for puromycin and cisplatin. *In vivo*, puromycin primarily affects the glomerular/mesangial cells, with significant nephrotoxicity *in vivo* thought to be caused by excessive protein reuptake secondary to serum protein leakage through damaged glomerular filters (Hjalmarsson, Ohlson and Haraldsson, 2001; Abbate, Zoja and Remuzzi, 2006). The organoids, being devoid of flowing blood, cannot flood nephrons with intraluminal protein, and therefore cannot produce this secondary damage. Damage to organoids is mainly expected to be via the primary targets (cells of the renal corpuscle including podocytes and mesangial cells). The extra sensitivity of 3D organoids to puromycin may well reflect the higher proportion of cells associated with the glomeruli such as podocytes in these compared to flat organoids (Takasato *et al.*, 2016; Hale *et al.*, 2018). Cisplatin is taken up mainly through the transporter OCT2 (SLC22A2). As presented in this paper, expression of this

transporter was weak in flat organoids and strong in 3D organoids, providing a possible explanation for the increased sensitivity of the latter to cisplatin. Ifosfamide is also taken up by the renal proximal tubule cells through the OCT2 (SLC22A2) transporter (Ciarimboli *et al.*, 2011), however, it is not possible to exclude its uptake by other cation transporters from that study. Ifosfamide may be taken up by other cation transporters such as OCTN1 that are present in the flat organoids, since we see a significant increase in fluorescence with this compound in those organoids. Nevertheless, the more robust increase in fluorescence in the 3D organoids for this compound after 24h probably reflects the involvement of OCT2 in the uptake of this compound.

Unlike the transporter-driven uptake of cisplatin and ifosfamide, gentamicin is taken up into proximal tubule cells through the combined actions of the endocytic proteins megalin and cubulin. Our RNA-seq analysis showed that these genes are expressed in flat organoids, and thus it is perhaps not surprising that the flat organoids as well as the 3D organoids were able to predict toxicity to this compound. The gentamicin-treated 3D organoids (but not flat ones) maintained their tubular structures in sharp contrast to the cisplatin-treated 3D organoids, in which distinct loss of tubular structure was observed especially at the higher concentrations (data not shown).

When flat and 3D organoids were treated with cidofovir, an increase in fluorescence was observed in flat organoids only after the longer incubation time of 72h. Cidofovir is taken up in the proximal tubule cells by organic anion transporters OAT1 and, to some extent, OAT3 (Uwai *et al.*, 2007). The low levels of these transporters in the flat organoids might explain the lack of fluorescence at the 24h time point, with increasing fluorescence only after a longer incubation as is seen with cisplatin. Cidofovir causes damage to tubular cells leading to induction of apoptosis, and *in vitro* studies typically require treatment of several days to induce damage (Ho *et al.*, 2000; Ortiz et al., 2005). Interestingly, the 3D organoids appeared to be relatively insensitive to the compound in terms of induction of oxidative stress and reporter

expression, despite the presence of the anion uptake transporter OAT1. Since cidofovir is more selectively toxic to proximal tubules than some of the other compounds tested, it may be that the lack of sensitivity of the 3D renal organoids to cidofovir reflects a more mixed combination of renal cell types, with fewer of them being of proximal tubule identity. The mechanism of cidofovir nephrotoxicity is currently unclear, and it is also important to note that both the flat and 3D renal organoids are closer to human embryonic kidneys than adult kidneys; this immaturity may account for some of the differences between responses. It is also of note that the single endpoint for this study (the fluorescence analysis of oxidative stress reporter) may not identify all toxicants, and that a combination of this assay and another endpoint may be more informative.

We conclude that the reporter-hiPSC-derived renal organoids can predict toxicity to kidneys (Figure 6), but that they are variable in their individual responses to compound treatment and that certain organoid formats (flat or 3D) may be better suited to different classes of drugs. Although the 3D organoids in general could predict toxicity at a lower concentration than the flat organoids, the response for the 3D organoids was generally slower than the flat organoids when assessing the 24h timepoint. This may reflect a difference in penetration of compounds in the 3D, dome-shaped organoids with their more densely packed renal structures compared to the flat organoids. In addition, some compounds required longer incubation to elicit a measurable response via the oxidative stress pathway, which may be explained by the different mechanisms of toxicity of these compounds. The inherent variability of the organoids may also play a part in these results and addressing this will be important for the future of organoids for high-throughput drug screening.

The fluorescence increases in response to application of varying concentrations of nephrotoxicants in these organoids requires a binary interpretation. These organoids represent a possible broad screening tool for nephrotoxic compounds, and further investigations may help to explain some

differences in compound responses and be an additional useful tool to identify mechanisms of toxicity.

Comparison of the *HO1*-mCherry-hiPSC reporter fluorescence, to qPCR analyses of *HMOX1* transcription in response to the same compounds (Figure S5 and Table S3), shows that there is broad agreement between the data. As mentioned previously, while the increases in fluorescence intensity and the transcript increases of *HMOX1* did not mirror each other exactly, this is likely due to the accumulation of fluorophore with a longer half-life (24h) (Snapp, 2009) (Shaner *et al.*, 2004) than the half-life of the transcripts. The fluorescence assay may provide a more sensitive response than qPCR for predicting toxicity and, additionally provides the option of multiple time points on the same samples as well as using fewer reagents and being less time-consuming.

Limitations

It is important to note that, while this system could identify toxicities, we do not claim on the strength of the data presented here that it will perform adequately on all possible nephrotoxicants. Rather, we propose it as one useful tool in screening, not as the only system needed. We also stress that a much larger set of compounds (both nephrotoxic and non-nephrotoxic) would have to be tested to validate the system and conclude on its predictive power. Our testing of 7 compounds and getting 7/7 correct calls (calls made when considering both flat and 3D organoids together, and regarding a signal in either as an indication of toxicity as explained in the last section of Results) is adequate as a proof of concept for engineering reporters into hiPSCs for nephrotoxicity testing, but this modest number of test compounds does not indicate that our test can be relied upon to be correct 100% of the time. The Wilson Score Interval method of calculating confidence intervals indicates that 7/7 correct calls provides 95% confidence of making a wrong call in no more than 44% of tests. The test cannot therefore be relied upon in real screening programmes

until it has been subjected to a much larger number of tests (by the Wilson Score Interval method, 94/94 correct calls would be needed to give a test a 95% confidence of making a false call in fewer than 5% of tests).

The differentiation of iPSC into organoids always carries the risk of producing off-target cells, neurons being particularly common contaminants in the case of kidney organoids. This raises the possibility of ‘false-positive’ indications of nephrotoxicity if the cells that express HMOX1 are of an off-target type, if cultures are read by simple machine-assessment of fluorescence rather than by microscopic observation. In the context of the intended application of this system – screening candidate compounds for toxicity that would see them fail clinical trials – ‘false positivity’ would not be a major problem because safe compounds should not cause severe stress to any cell type. If neurons, for example, in a renal culture, gave a ‘false-positive’ because in fact the compound was toxic to brain rather than kidney, the overall effect would still be that a potentially dangerous compound was detected before it went forward and caused problems.

The system we describe gives no direct indication of mechanism beyond the presence of oxidative stress somewhere in the organoid. This is sufficient for giving a warning about a test compound, but is of limited help in guiding researchers towards possible strategies for mitigation, either through chemical modification of the compound or co-administration of an uptake-channel inhibitor. These steps would be assisted by establishing which cells of the kidney are (worst) affected by the toxicant. This could be done by sectioning and staining the organoids (which are rather too thick for clear imaging as they are) for HMOX1 and cell- or segment-specific markers. It could also be done by disaggregating the organoid, separating its cells by FACS, and analyzing each population for specific types of damage or even to a complete transcriptomic study if the importance of the test compound warranted that investment. However, given the limitations of organoids in terms of maturity, cultured primary cells or tissues (for example, from potential transplant kidney that could not be used) would probably be a much more informative system in

which to follow up mechanisms of toxicity of a compound worth the effort, once toxicity had been indicated by the simple screen described in this report. We are not in any way claiming that the system described here can yield high-resolution mechanistic data; rather, that it can provide a simple indication of potential danger (to offer an analogy: it is a smoke alarm, not a mass spectrometer).

Conclusion

Subject to the limitations discussed in the forgoing section, we have demonstrated an effective organoid-based test for nephrotoxicity by oxidative stress that features an easy to read, built-in fluorescent reporter system. Although we differentiated our cells towards the renal lineage, as a global marker of oxidative stress, a reporter for *HMOX1* expression in human pluripotent cells will be an invaluable tool for a broad range of applications in other organoids and engineered tissues.

Acknowledgements

This work was supported by the Medical Research Council (MRC) grants MR/K010735/1, MR/R026483/1, Kidney Research UK grant RP_002_20160223, The University of Edinburgh ISSF3 grant (IS30R35) and the Biotechnology and Biological Sciences Research Council (BBSRC; grant number BB/P013732/1). ME was supported by a scholarship from the Egyptian Ministry of Higher Education and Scientific Research, Cultural Affairs and Missions sector. This research was funded in whole, or in part, by the Wellcome Trust [Grant number IS30R35]. For the purpose of open access, the author has applied a CC BY public copyright licence to any Author Accepted Manuscript version arising from this submission".

Declaration of Interests

The authors declare no competing interests.

Author Contributions

Conceptualization, M.L.L., P.H., AK.S., M.E., J.A.D.; Methodology, M.L.L., M.E., W.L., AK.S.; Investigation, M.L.L., M.E., W.L., S.L., A.P, L.S., M.M.;

Writing – Original Draft, M.L.L., M.E., J.A.D.; Writing – Review & Editing, M.L.L, M.E., M.M., W.L., S.L., P.H., AK.S, J.A.D.; Formal Analysis, M.L.L. and M.E.; Visualization, M.L.L.; Project Administration, M.L.L., Funding Acquisition, M.L.L. and J.A.D.; Resources, AK.S and J.A.D., Supervision, AK.S and J.A.D.

References

Abbate, M., Zoja, C. and Remuzzi, G. (2006) 'How Does Proteinuria Cause Progressive Renal Damage?', *Journal of the American Society of Nephrology*, 17(11), pp. 2974–2984. doi: 10.1681/ASN.2006040377.

Adler, M. *et al.* (2016) 'A Quantitative Approach to Screen for Nephrotoxic Compounds In Vitro.', *Journal of the American Society of Nephrology : JASN*. American Society of Nephrology, 27(4), pp. 1015–28. doi: 10.1681/ASN.2015010060.

Akilesh, S. *et al.* (2014) 'Chronic Ifosfamide Toxicity: Kidney Pathology and Pathophysiology', *American Journal of Kidney Diseases*, 63(5), pp. 843–850. doi: 10.1053/j.ajkd.2013.11.028.

Archibald, K., Coleman, R. and Foster, C. (2011) 'Open letter to UK Prime Minister David Cameron and Health Secretary Andrew Lansley on safety of medicines.', *Lancet (London, England)*, 377(9781), p. 1915. doi: 10.1016/S0140-6736(11)60802-7.

Armstrong, J. F. *et al.* (1993) 'The expression of the Wilms' tumour gene, WT1, in the developing mammalian embryo.', *Mechanisms of development*, 40(1–2), pp. 85–97.

Bajaj, P. *et al.* (2018) 'Human Pluripotent Stem Cell-Derived Kidney Model for Nephrotoxicity Studies.', *Drug metabolism and disposition: the biological fate of chemicals*. American Society for Pharmacology and Experimental Therapeutics, 46(11), pp. 1703–1711. doi: 10.1124/dmd.118.082727.

Barnett, L. M. A. and Cummings, B. S. (2018) 'Nephrotoxicity and Renal Pathophysiology: A Contemporary Perspective', *Toxicological Sciences*. Narnia, 164(2), pp. 379–390. doi: 10.1093/toxsci/kfy159.

Barresi, G., Tuccari, G. and Arena, F. (1988) 'Peanut and Lotus tetragonolobus binding sites in human kidney from congenital nephrotic syndrome of Finnish type.', *Histochemistry*, 89(2), pp. 117–20.

Baverel, G. *et al.* (2013) 'Use of precision-cut renal cortical slices in nephrotoxicity studies.', *Xenobiotica; the fate of foreign compounds in biological systems*, 43(1), pp. 54–62. doi: 10.3109/00498254.2012.725142.

Çetinkaya, I. *et al.* (2003) 'Regulation of human organic cation transporter

hOCT2 by PKA, PI3K, and calmodulin-dependent kinases', *American Journal of Physiology - Renal Physiology*. American Physiological Society, 284(2), pp. F293–F302. doi: 10.1152/AJPRENAL.00251.2002.
Cheng, Y.-T. *et al.* (2014) 'DJ-1 plays an important role in caffeic acid-mediated protection of the gastrointestinal mucosa against ketoprofen-induced oxidative damage', *The Journal of Nutritional Biochemistry*, 25(10), pp. 1045–1057. doi: 10.1016/j.jnutbio.2014.05.007.
Chu, X., Bleasby, K. and Evers, R. (2013) 'Species differences in drug transporters and implications for translating preclinical findings to humans', *Expert Opinion on Drug Metabolism & Toxicology*. Taylor & Francis, 9(3), pp. 237–252. doi: 10.1517/17425255.2013.741589.
Ciarimboli, G. *et al.* (2011) 'New Clues for Nephrotoxicity Induced by Ifosfamide: Preferential Renal Uptake via the Human Organic Cation Transporter 2', *Molecular Pharmaceutics*, 8(1), pp. 270–279. doi: 10.1021/mp100329u.
Davies, J. and Lawrence, M. (2018) *Organs and Organoids.* 1st edn. Edited by J. Davies and M. Lawrence. Academic Pr.
Fletcher, A. P. (1978) 'Drug Safety Tests and Subsequent Clinical Experience', *Journal of the Royal Society of Medicine*, 71(9), pp. 693–696. doi: 10.1177/014107687807100915.
Hale, L. J. *et al.* (2018) '3D organoid-derived human glomeruli for personalised podocyte disease modelling and drug screening', *Nature Communications*, 9(1). doi: 10.1038/s41467-018-07594-z.
Hartung, T. (2009) 'Toxicology for the twenty-first century', *Nature*, 460(7252), pp. 208–212. doi: 10.1038/460208a.
Hennigar, R. A., Schulte, B. A. and Spicer, S. S. (1985) 'Heterogeneous distribution of glycoconjugates in human kidney tubules', *The Anatomical Record*, 211(4), pp. 376–390. doi: 10.1002/ar.1092110403.
Hjalmarsson, C., Ohlson, M. and Haraldsson, B. (2001) 'Puromycin aminonucleoside damages the glomerular size barrier with minimal effects on charge density', *American Journal of Physiology-Renal Physiology*, 281(3), pp. F503–F512. doi: 10.1152/ajprenal.2001.281.3.F503.
Ho, E. S. *et al.* (2000) *Cytotoxicity of Antiviral Nucleotides Adefovir and*

Cidofovir Is Induced by the Expression of Human Renal Organic Anion Transporter 1.
Huang, J. X. *et al.* (2015) 'Evaluation of biomarkers for in vitro prediction of drug-induced nephrotoxicity: comparison of HK-2, immortalized human proximal tubule epithelial, and primary cultures of human proximal tubular cells.', *Pharmacology research & perspectives*. Wiley-Blackwell, 3(3), p. e00148. doi: 10.1002/prp2.148.
Huch, M. *et al.* (2017) 'The hope and the hype of organoid research', *Development*, 144(6), pp. 938–941. doi: 10.1242/dev.150201.
Jang, K.-J. *et al.* (2013) 'Human kidney proximal tubule-on-a-chip for drug transport and nephrotoxicity assessment.', *Integrative biology : quantitative biosciences from nano to macro*, 5(9), pp. 1119–29. doi: 10.1039/c3ib40049b.
Jenkinson, S. E. *et al.* (2012) 'The limitations of renal epithelial cell line HK-2 as a model of drug transporter expression and function in the proximal tubule', *Pflügers Archiv - European Journal of Physiology*, 464(6), pp. 601–611. doi: 10.1007/s00424-012-1163-2.
Jun, D. *et al.* (2018) 'Tubular organotypic culture model of human kidney', *PLOS ONE*. Edited by J. Rajasingh. Public Library of Science, 13(10), p. e0206447. doi: 10.1371/journal.pone.0206447.
Karatas, Y. *et al.* (2004) 'Effect of tempol (4-hydroxy tempo) on gentamicin-induced nephrotoxicity in rats', *Fundamental and Clinical Pharmacology*. John Wiley & Sons, Ltd (10.1111), 18(1), pp. 79–83. doi: 10.1046/j.0767-3981.2003.00211.x.
Kim, D. and Dressler, G. R. (2005) 'Nephrogenic factors promote differentiation of mouse embryonic stem cells into renal epithelia.', *Journal of the American Society of Nephrology : JASN*, 16(12), pp. 3527–34. doi: 10.1681/ASN.2005050544.
Knight, A. (2008) 'Systematic reviews of animal experiments demonstrate poor contributions toward human healthcare.', *Reviews on recent clinical trials*, 3(2), pp. 89–96.
Kohli, H. S. *et al.* (2000) 'Treatment-related acute renal failure in the elderly: a hospital-based prospective study.', *Nephrology, dialysis, transplantation : official publication of the European Dialysis and Transplant Association -*

European Renal Association, 15(2), pp. 212–7.
Kreidberg, J. A. *et al.* (1993) 'WT-1 is required for early kidney development.', *Cell*, 74(4), pp. 679–91.
Lawrence, M. L., Chang, C.-H. and Davies, J. A. (2015) 'Transport of organic anions and cations in murine embryonic kidney development and in serially-reaggregated engineered kidneys', *Scientific Reports*, 5, p. 9092. doi: 10.1038/srep09092.
Lee, S.-Y. *et al.* (2013) 'Expression of E-cadherin in pig kidney.', *Journal of veterinary science*, 14(4), pp. 381–6.
van Leeuwen, J. S. *et al.* (2012) 'Differential involvement of mitochondrial dysfunction, cytochrome P450 activity, and active transport in the toxicity of structurally related NSAIDs', *Toxicology in Vitro*. Pergamon, 26(2), pp. 197–205. doi: 10.1016/J.TIV.2011.11.013.
Li, W. *et al.* (2003) 'Use of cultured cells of kidney origin to assess specific cytotoxic effects of nephrotoxins', *Toxicology in Vitro*, 17(1), pp. 107–113. doi: 10.1016/S0887-2333(02)00128-5.
Li, Y. *et al.* (2013) 'An in vitro method for the prediction of renal proximal tubular toxicity in humans', *Toxicology Research*. doi: 10.1039/c3tx50042j.
Mehta, R. L. *et al.* (2004) 'Spectrum of acute renal failure in the intensive care unit: the PICARD experience.', *Kidney international*, 66(4), pp. 1613–21. doi: 10.1111/j.1523-1755.2004.00927.x.
Mi, H. *et al.* (2017) 'PANTHER version 11: expanded annotation data from Gene Ontology and Reactome pathways, and data analysis tool enhancements', *Nucleic Acids Research*. Oxford University Press, 45(D1), pp. D183–D189. doi: 10.1093/nar/gkw1138.
Mikkaichi, T. *et al.* (2004) 'Isolation and characterization of a digoxin transporter and its rat homologue expressed in the kidney.', *Proceedings of the National Academy of Sciences of the United States of America*, 101(10), pp. 3569–74. doi: 10.1073/pnas.0304987101.
Miller, R. P. *et al.* (2010) 'Mechanisms of Cisplatin nephrotoxicity.', *Toxins*. Multidisciplinary Digital Publishing Institute (MDPI), 2(11), pp. 2490–518. doi: 10.3390/toxins2112490.
Morales, A. I. *et al.* (2010) 'Metformin prevents experimental gentamicin-

induced nephropathy by a mitochondria-dependent pathway.', *Kidney international*. Elsevier, 77(10), pp. 861–9. doi: 10.1038/ki.2010.11.
Morizane, R. *et al.* (2015) 'Nephron organoids derived from human pluripotent stem cells model kidney development and injury', *Nature Biotechnology*, 33(11). doi: 10.1038/nbt.3392.
El Mouedden, M. *et al.* (2000) 'Gentamicin-induced apoptosis in renal cell lines and embryonic rat fibroblasts.', *Toxicological sciences : an official journal of the Society of Toxicology*, 56(1), pp. 229–39.
Newcombe, R. G. (1998) 'Two-sided confidence intervals for the single proportion: comparison of seven methods.', *Statistics in medicine*, 17(8), pp. 857–72.
Ortiz, Alberto; Justo, Pilar; Sanz, Ana; Melero, Rosa; Caramelo, Carlos; Guerrero, Manuel Fernandez; Strutz, Frank; Muller, Gerhard; Borat, Antonio; Egido, J. (2005) 'Tubular cell apoptosis and cidofovir-induced acute renal failure', *Antiviral Therapy*, 10, pp. 185–190.
Przepiorski, A. *et al.* (2018) 'A Simple Bioreactor-Based Method to Generate Kidney Organoids from Pluripotent Stem Cells.', *Stem cell reports*, 11(2), pp. 470–484. doi: 10.1016/j.stemcr.2018.06.018.
Regec, A. L., Trifillis, A. L. and Trump, B. F. (1986) *The Effect of Gentamicin on Human Renal Proximal Tubular Cells**, *SYMPOSIUM Renal Pathology and Toxicity TOXICOLOGIC PATHOLOGY ISSNO192-6233*.
Regec, A. L., Trump, B. F. and Trifilis, A. L. (1989) 'Effect of gentamicin on the lysosomal system of cultured human proximal tubular cells: Endocytotic activity, lysosomal pH and membrane fragility', *Biochemical Pharmacology*. Elsevier, 38(15), pp. 2527–2534. doi: 10.1016/0006-2952(89)90098-1.
Schmitz, C. *et al.* (2002) 'Megalin Deficiency Offers Protection from Renal Aminoglycoside Accumulation', *Journal of Biological Chemistry*, 277(1), pp. 618–622. doi: 10.1074/jbc.M109959200.
Shaner, N. C. *et al.* (2004) 'Improved monomeric red, orange and yellow fluorescent proteins derived from Discosoma sp. red fluorescent protein', *Nature Biotechnology*. doi: 10.1038/nbt1037.
Sjögren, A.-K. *et al.* (2018) 'A novel multi-parametric high content screening assay in ciPTEC-OAT1 to predict drug-induced nephrotoxicity during drug

discovery', *Archives of Toxicology*. Springer Berlin Heidelberg, 92(10), pp. 3175–3190. doi: 10.1007/s00204-018-2284-y.
Snapp, E. L. (2009) 'Fluorescent proteins: a cell biologist's user guide', *Trends in Cell Biology*, 19(11), pp. 649–655. doi: 10.1016/j.tcb.2009.08.002.
Takasato, M. *et al.* (2015) 'Kidney organoids from human iPS cells contain multiple lineages and model human nephrogenesis', *Nature*, 526(7574). doi: 10.1038/nature15695.
Takasato, M. *et al.* (2016) 'Generation of kidney organoids from human pluripotent stem cells.', *Nature protocols*, 11(9). doi: 10.1038/nprot.2016.098.
Tsuda, M. *et al.* (2007) 'Oppositely directed H+ gradient functions as a driving force of rat H+/organic cation antiporter MATE1', *American Journal of Physiology - Renal Physiology*, 292(2).
Uchino, S. *et al.* (2005) 'Acute renal failure in critically ill patients: a multinational, multicenter study.', *JAMA*, 294(7), pp. 813–8. doi: 10.1001/jama.294.7.813.
Uwai, Y. *et al.* (2007) 'Renal transport of adefovir, cidofovir, and tenofovir by SLC22A family members (hOAT1, hOAT3, and hOCT2).', *Pharmaceutical research*, 24(4), pp. 811–5. doi: 10.1007/s11095-006-9196-x.
Weber, E. J. *et al.* (2016) 'Development of a microphysiological model of human kidney proximal tubule function.', *Kidney international*, 90(3), pp. 627–37. doi: 10.1016/j.kint.2016.06.011.
Xinaris, C., Brizi, V. and Remuzzi, G. (2015) 'Organoid Models and Applications in Biomedical Research', *Nephron*, 130(3), pp. 191–199. doi: 10.1159/000433566.
Zou, L. *et al.* (2018) 'Molecular Mechanisms for Species Differences in Organic Anion Transporter 1, OAT1: Implications for Renal Drug Toxicity.', *Molecular pharmacology*. American Society for Pharmacology and Experimental Therapeutics, 94(1), pp. 689–699. doi: 10.1124/mol.117.111153.

Figure 1

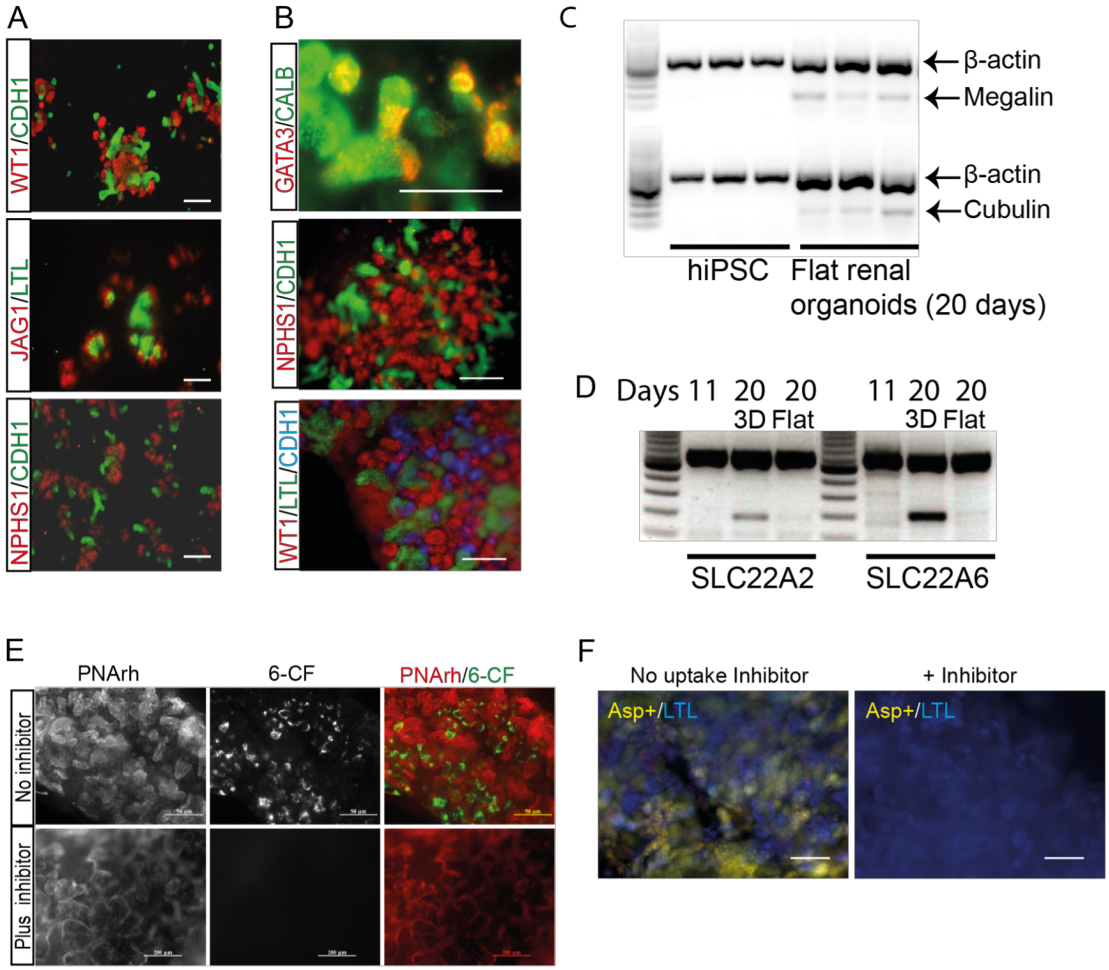

Figure 1 - Renal organoids express renal markers and display some renal functions

A) Flat renal organoids express the renal mesenchymal and collecting duct markers WT1 and CDH1, podocyte marker NPHS1, and the nephron marker JAG1, as well as binding the proximal tubule (PT) marker lotus tetragonolobus lectin (LTL). B) 3D renal organoids express markers of ureteric-bud tips (GATA3), collecting duct (CALB, CDH1), podocytes (WT1, NPHS1) and bind the PT marker LTL. C) In contrast to undifferentiated hiPSCs, flat renal organoids express *Megalin* and *Cubulin* as measured by RT-PCR with three biological replicates each (3 different hiPSC samples and 3 flat organoids). D) Expression of the renal anion and cation uptake transporters *OCT2 (SLC22A2)* and *OAT1 (SLC22A6)* in flat and 3D renal organoids by RT-PCR. E) Specific tubular uptake of the fluorescent anion 6-CF (green) in 3D renal

organoids stained with the live tubular marker rhodamine-peanut agglutinin (PNArh, red) either with or without the anion transporter inhibitor probenecid. F) Specific tubular uptake of the fluorescent cation 4-(4-dimethylamino-styryl)-N-methylpyridinium iodide (Asp+, yellow) stained with the renal tubular marker lotus tetragonolobus lectin (LTL, blue) either with or without the cation transporter inhibitor TPA. Scale bars are 100μm (A); 200 μm (B, top panel) and (E); 50μm (B, middle and bottom panel) and (F). Unlabelled tracks on RT-PCR gels are molecular weight markers.

Figure 2

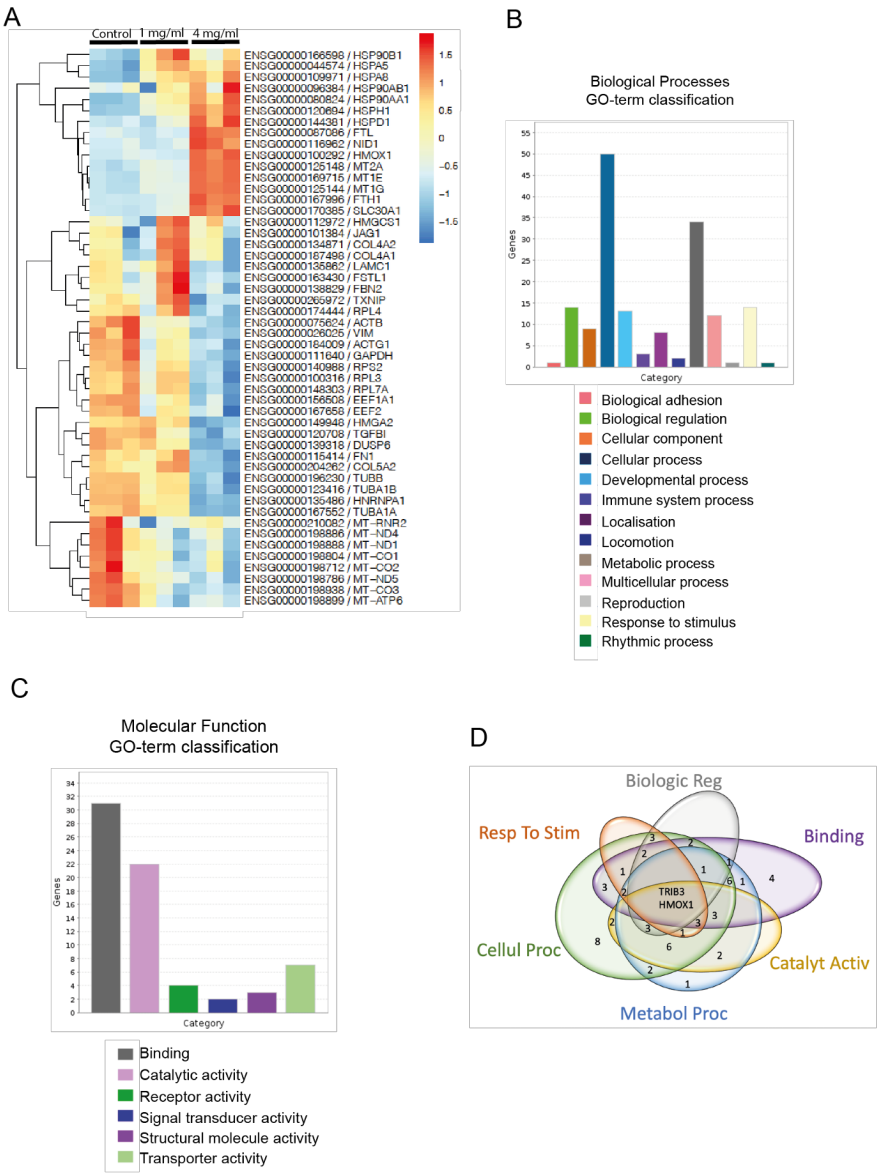

Figure 2 – RNA-seq analyses of hiPSC-derived flat renal organoids

A) RNA-seq analyses of wild type hiPSC-derived flat renal organoids treated with gentamicin (1mg/ml or 4mg/ml) or left untreated. Heat-map shows top 50 most differentially expressed genes among all three groups. The heat-map of each row is defined independently to span the highest and lowest normalized expression of that row (-1.5 (lowest) to 1.5 (highest)) thus showing the variability of that specific gene between the samples. B) Gene ontology (GO) classification of the top 100 up-regulated genes comparing the samples treated with the highest concentration with untreated samples (filtered first by

lowest FDR and then top 100 genes with highest-fold increases) for Biological Processes or C) Molecular Function. D) The Venn diagram shows overlaps of genes within the 6 largest functional GO classifications.

Figure 3

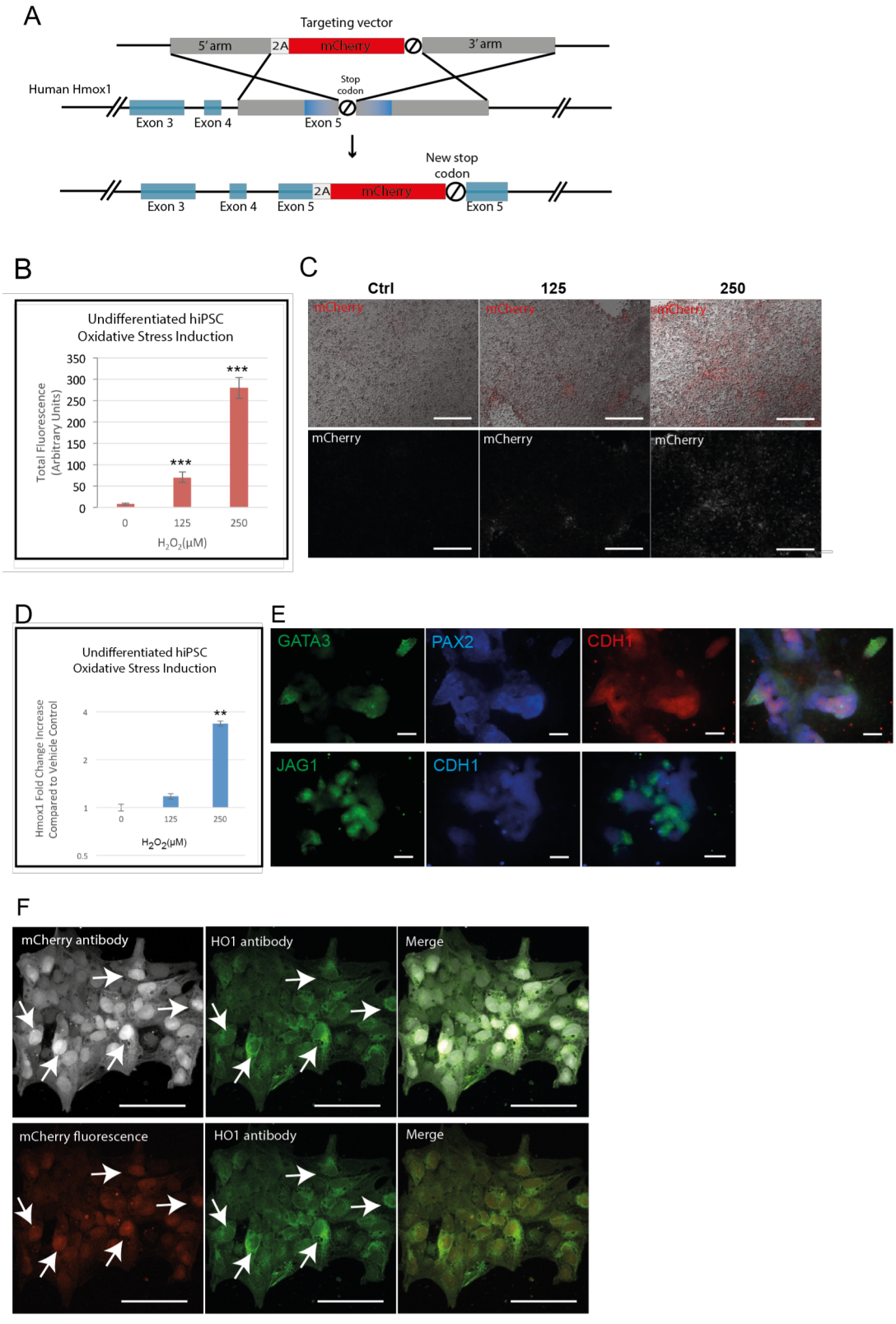

2

3 Figure 3 – Construction and verification of *HMOX1* reporter hiPSCs

A) Targeting vector diagram showing insertion of 2A peptide-mCherry-STOP sequence replacing endogenous stop codon of human *HMOX1* in hiPSCs using CRISPR gene editing. Homologous arms upstream (5': 500bp) and downstream (3': 1049bp) of the stop codon are shown in grey.
B) Increase in mCherry expression in undifferentiated *HO1*-mCherry-hiPSCs after induction of oxidative stress with hydrogen peroxide by measuring total fluorescence and C) representative images. Scale bars are 200µm. D) *HMOX1* transcript increase in undifferentiated *HO1*-mCherry-hiPSCs after induction of oxidative stress (by qPCR). E) *HO1*-mCherry-hiPSC differentiated flat renal organoids express nephron markers (GATA3, PAX2, CHD1, JAG1) and form renal structures. Scale bars are 100µm. F) Cellular co-expression of HO-1 and mCherry in undifferentiated hiPSCs after induction of oxidative stress with hydrogen peroxide (150µM), either using anti-HMOX1 and anti-mCherry antibodies (top panel) or anti-HMOX1 antibody together with reporter mCherry fluorescence (bottom panel). Scale bars are 100µM. In all graphs, data are represented as mean +/- SEM, and $p<0.05$ is indicated with (*), $p<0.01$ with (**) and $p<0.001$ with (***)

Figure 4

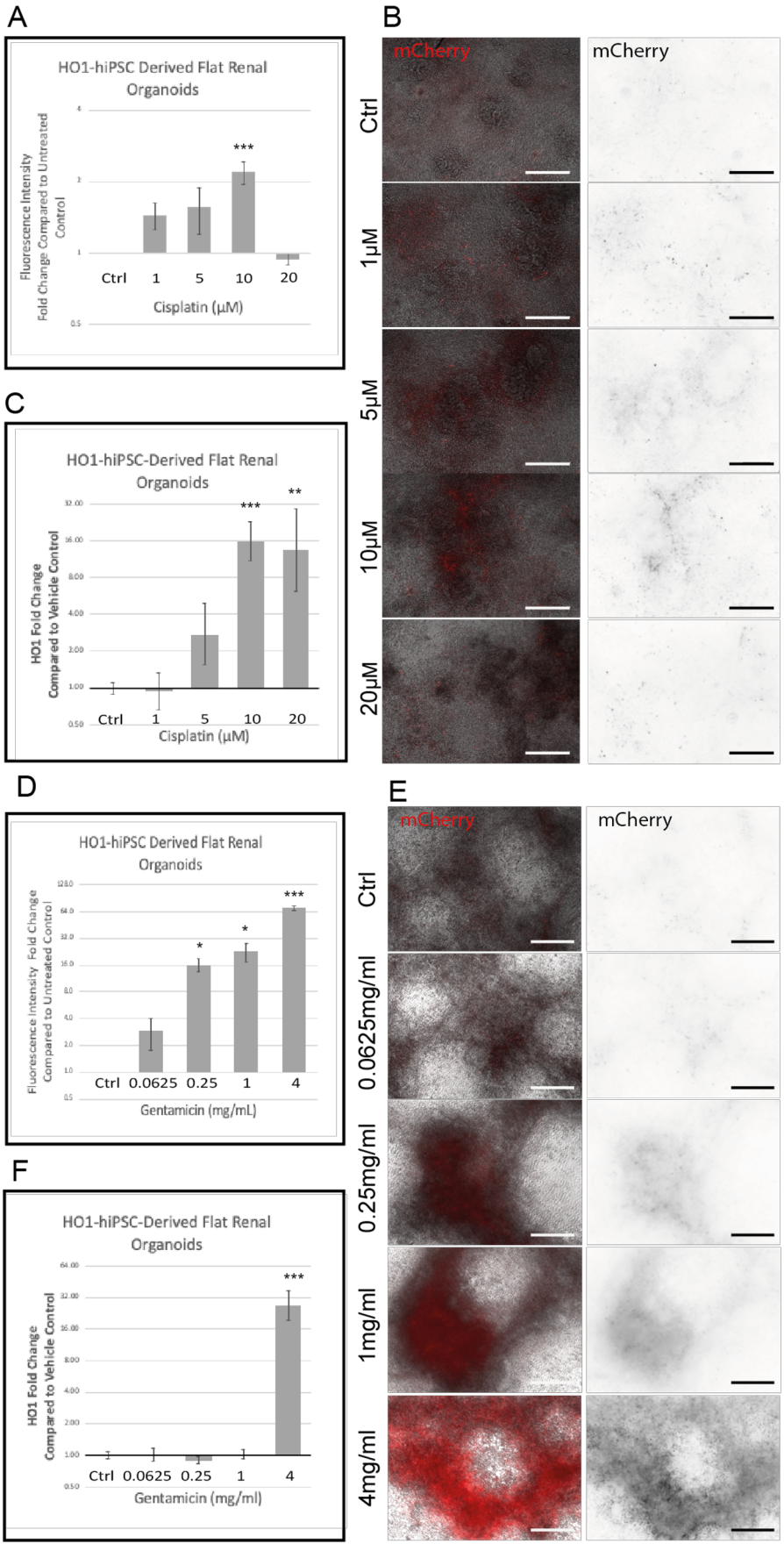
A
HO1-hiPSC Derived Flat Renal Organoids
Fluorescence Intensity Fold Change Compared to Untreated Control
***
Ctrl 1 5 10 20
Cisplatin (μM)
B
mCherry
mCherry
Ctrl
1μM
5μM
10μM
20μM
C
HO1-hiPSC-Derived Flat Renal Organoids
HO1 Fold Change Compared to Vehicle Control
***
**
Ctrl 1 5 10 20
Cisplatin (μM)
D
HO1-hiPSC Derived Flat Renal Organoids
Fluorescence Intensity Fold Change Compared to Untreated Control
*
*
***
Ctrl 0.0625 0.25 1 4
Gentamicin (mg/mL)
E
mCherry
mCherry
Ctrl
0.0625mg/ml
0.25mg/ml
1mg/ml
4mg/ml
F
HO1-hiPSC-Derived Flat Renal Organoids
HO1 Fold Change Compared to Vehicle Control
***
Ctrl 0.0625 0.25 1 4
Gentamicin (mg/ml)

Response of *HO1*-mCherry-hiPSC reporter-derived flat organoids to nephrotoxicants

Increase (fold-change relative to vehicle control) in mCherry expression in *HO1*-mCherry-hiPSC-derived flat renal organoids treated with cisplatin (A) or gentamicin (D) and representative images for cisplatin (B) or gentamicin (E). Scale bars are 200µm. *HMOX1* transcript increase (by qPCR) in *HO1*-mCherry-hiPSC-derived flat renal organoids treated with cisplatin (C) or gentamicin (F). qPCRs are fold-change relative to vehicle control. Data are represented as mean +/- SEM, $p<0.05$ is indicated with (*), $p<0.01$ with (**) and $p<0.001$ with (***)

Figure 5

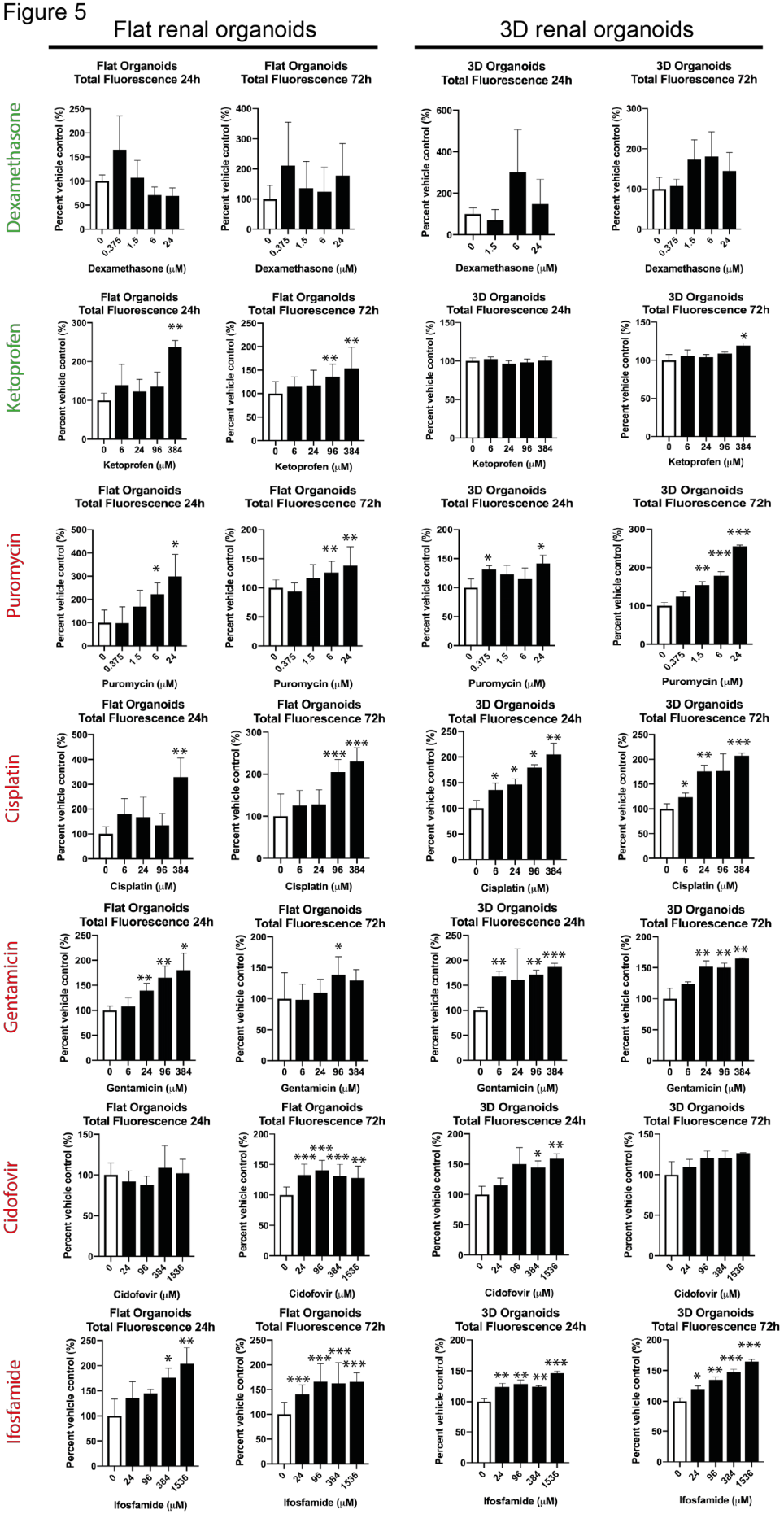
Flat renal organoids
3D renal organoids
Flat Organoids Total Fluorescence 24h
Flat Organoids Total Fluorescence 72h
3D Organoids Total Fluorescence 24h
3D Organoids Total Fluorescence 72h
Dexamethasone
Ketoprofen
Puromycin
Cisplatin
Gentamicin
Cidofovir
Ifosfamide
Percent vehicle control (%)
Dexamethasone (μM)
Ketoprofen (μM)
Puromycin (μM)
Cisplatin (μM)
Gentamicin (μM)
Cidofovir (μM)
Ifosfamide (μM)

Figure 5 – Response of HO1-mCherry-hiPSC-derived flat and 3D organoids to blinded compound screen.

Blind-coded compounds were used to treat *HO1*-mCherry-hiPSC derived renal organoids in either flat (left two panels) or 3D (right two panels) organoid forms, for either 24h or 72h, followed by measurements of fluorescence. Results are total fluorescence as a percent of the vehicle control. Significance of fluorescence intensity increase compared to the vehicle control was assessed using a T-test with Welch's correction. Each time-point and organoid format (flat or 3D) was carried out as a separate experiment and each included a vehicle-only control. Data are represented as mean +/- SEM, $p<0.05$ is indicated with (*), $p<0.01$ with (**) and $p<0.001$ with (***).

Table 1:

Compound	Flat 24h	Flat 72h	3D 24h	3D 72h
Dexamethasone	N	N	N	N
Ketoprofen	Y	Y	N	N
Puromycin	N	Y	N	Y
Cisplatin	Y	Y	Y	Y
Gentamicin	Y	N	Y	Y
Cidofovir	N	Y	Y	N
Ifosfamide	Y	Y	Y	Y

Figure 6 – Prediction of Toxicity by Increase in Fluorescence Intensity

N = Did not predict toxicity, Y = Did predict toxicity. Green indicates results that are consistent with known clinical data. Prediction score is based on data in Figure 4. A p value of 0.01 or more for one or more of the treatment concentrations is designated as having predicted toxicity.

STAR methods

RESOURCE AVAILABILITY

Lead contact

Further information and requests for resources and reagents should be directed to and will be fulfilled by the lead contact, Jamie Davies (jamie.davies@ed.ac.uk).

Materials availability

The HO1-mCherry-hiPSC oxidative stress reporter cell line generated in this study is available in Jamie Davies' lab, Edinburgh University, and can be obtained upon request.

Data and code availability

- RNA-seq data are publicly available in GEO (GSE195642)
- This study did not generate novel computer code/ software
- Image sets will appear on acceptance at DataShare@ed.ac.uk and will be publicly available and can be located by searching on the title of this paper.

Any additional information required to reanalyze the data reported in this paper is available from the lead contact upon request.

EXPERIMENTAL MODEL AND SUBJECT DETAILS

hiPSC line and maintenance

hiPS cells (clone AD3-01, derived from adult human dermal fibroblasts) were plated on Matrigel-coated plates and cultured in Essential 8 (E8) medium at 37°C in 5% CO_2. When they had reached 80% confluence, cells were treated for 1 hour with the ROCK inhibitor Y-27632 (10μM) then were dissociated in 0.5 mM EDTA in PBS and plated on Matrigel-coated plates. The culture medium was supplemented with ROCK inhibitor (10μM) for the first 24 hours. Media were changed daily, with changes having no ROCK inhibitor.

METHOD DETAILS

Production of hiPSC-derived renal organoids

Pluripotency was affirmed in our starting population of hiPSCs by immunostaining for the pluripotency markers Oct3/4 and Nanog, and positive staining for Alkaline Phosphatase (Figure S1A). An established protocol (Takasato *et al.*, 2015), with minor modifications (Figure S1B), was applied to the hiPSCs to induce renal differentiation via a path that differentiates hiPSC first to a primitive streak-like identity, then to an intermediate mesoderm-like identity and finally to the precursors of renal development: ureteric bud and metanephric mesenchyme. After 2 days of CHIR99201 treatment, Oct3/4 expression was replaced by the expression of primitive streak marker, Brachyury (Figure S1C left panel). After a further 2 days of CHIR99201, cells were treated with FGF9 and heparin to induce differentiation towards the intermediate mesoderm (IM) fate. By day 5 of the treatment with FGF9 and heparin the cells expressed LHX1 and PAX2, markers of IM (Figure S1C right panel). After 12 days in total, exogenous FGF9 and heparin were withdrawn and the cells continued to differentiate towards renal fate. By day 18 of differentiation bundles of tubules could be seen in flat organoids, which spread across the bottom of a well (Figure S1D). To make 3D organoids, undifferentiated cells were cultured as above in six-well plates (144,000 cells/ well) until 7 days after starting differentiation, when each well was dissociated using Trypsin/ EDTA, and pelleted at 300,000 cells/pellet. (Figure S1E). Pellets were grown on the surface of transwell inserts with medium added to the lower compartment only. 10μM Y-27632 was added to the culture media for overnight after dissociation and was removed afterwards. The re-aggregated pellets were treated with Heparin (1μg/ml) and FGF9 (200ng/ml) for a further 5 days, then were withdrawn and no further growth factors were given. Differentiation was complete by 18 days, and resulted in dome-shaped organoids with robust and dense tubule development (Figure S1F).

CRISPR-Cas9 editing of HMOX1 gene in hiPSCs

We designed a targeting vector containing a 2A-peptide-mCherry-STOP cassette flanked by homologous 5' and 3' arms upstream (500bp) and downstream (1049bp) of the endogenous stop codon of the endogenous *HMOX1* gene in the hiPSCs (Figure 3A). The targeting sequence was synthesized by Integrated DNA Technologies and then subcloned into pUC18 for transfection. Guide RNAs (gRNAs) were designed using the Zhang lab resource) (Table S4). Undifferentiated hiPSCs were co-transfected in equimolar amounts with the Cas9-GFP (pCas9_GFP; Addgene) and gRNA plasmids together with the targeting vector containing the repair template. After letting the cells recover and proliferate for 72h, cells were treated with hydrogen peroxide to induce oxidative stress (0, 25 or 150μM) and then sorted using FACS to isolate the mCherry-targeted population (Figure S4A). Wild type hiPSCs were used as a control for gating. The enriched populations were recovered and expanded for a further 7 days. To isolate clonal populations of targeted hiPSCs, we again used FACS. The low but detectable basal level of HMOX1 expression in undifferentiated hiPSCs allowed us to sort single, weakly mCherry-positive hiPSCs into wells of a 96-well plate without needing to first induce oxidative stress (Figure S4B). Wild type hiPSCs (AD3-01) were again used for gating. After a further 7 days, 24 clonal populations from the single-cells sorted by FACS had survived and expanded. These were further expanded into individual wells of a 6-well plate. PCR, using primers designed to span the targeted region (Supplementary Table 4), was used to confirm that the reporter cassette had been integrated (Figure S4C primers 1 and 4). The product size without cassette insertion is 1654bp, whereas product size with insertion is 2428bp (Figure S4D), as expected. Clones were sequenced using primers spanning the homologous arms and inserted cassette (primers 1 and 2 at 5' end and primers 3 and 4 at 3' end) (Supplementary Table 4).

RT-PCR and qPCR

Total RNA was isolated from organoids using the Qiagen RNeasy mini kit. Flat organoids were dissociated and processed as per the kit protocol. 3D organoids were lysed using the lysis buffer provided in the kit and then

passed through a needle to fully dissociate before continuing with the kit protocol. RNA was stored at -80°C until use. cDNA for qPCR was prepared using 2μg RNA and cDNA for RT-PCR was prepared using 1μg of RNA. All cDNA was quality-controlled by PCR using intron-spanning primers for β-actin on cDNA, prepared with or without reverse transcriptase (primers in Supplementary Table 4). RT-PCRs for *OAT1 (SLC22A6)* and *OCT2 (SLC22A2)* were carried out in multiplex reactions with primers for β-actin as loading controls (primers in Supplementary Table 4). qPCRs on undifferentiated and flat organoids for *HMOX1* with *HPRT1* as internal control were performed using TaqMan reagents as per published protocols (Applied Biosystems, assay nos. in Supplementary Table 4). For qPCRs in the blind-coded screen, quality-controlled cDNA was provided by the Edinburgh authors to the Gothenburg authors. 12 ng of cDNA was utilized for each qPCR reaction. TaqMan gene expression assays (Applied Biosystems, TaqMan Gene Expression FAST Master Mix) were performed on HMOX1 and house-keeping genes HPRT and RPLP0. The reaction was prepared via Beckman NX and measured on Applied Biosystems QuantStudio 7 Real-Time PCR System.Technical triplicates served to calculate CT mean for each gene. The ΔCT between the target gene and the mean CT of the two reference genes was calculated for each biological replicate. The mean ΔCT of biological triplicates was normalized to untreated sample resulting in $2^{\Delta\Delta CT}$. The square root of vehicle and treated sample variance resulted in the standard deviation of ΔCT treated sample. A one-way ANOVA on repeated measures was performed. Significant fold-change was established by Dunnett's multiple comparisons test.

RNA-seq analysis

RNA-seq, and trimming, filtering and normalization of raw data, was performed by Edinburgh Genomics. 1 μg of total RNA/sample was used for sequencing library preparation using an Illumina TruSeq stranded mRNA kit. Sequencing was performed using a Novaseq S1 50 Paired-end run to produce 50-64 million read-pairs per sample. Reads were trimmed using Cutadapt and were aligned to the *Homo sapiens* reference genome (GRCh38;

from Ensembl) using STAR. Standard GTF-format annotation for the reference genome (annotation version 84) was used. Reads were assigned to features of type 'exon' in the input annotation grouped by gene_id in the reference genome using Feature Counts. The raw count data were filtered to remove very low-expressed genes (genes consisting predominantly of near-zero counts), filtering was performed on counts per million to avoid artefacts due to library depth. Reads were normalised using the weighted trimmed mean of M-values method. Differential analysis (comparing the low-treated group to the control group, or the high-treated group to the control group) was carried out using edgeR4. Fold-changes were estimated as per the default behavior of edgeR, to avoid artefacts which occur with empirical calculation. Statistical assessment of differential expression was carried out with the quasi-likelihood (QL) F-test.

To analyse the up-regulated genes in the high-treated versus the control contrast, we first selected the 400 genes with the lowest *p* value corrected for FDR, then from these picked the 100 most strongly up-regulated and used them for downstream analysis. We performed a PANTHER Overrepresentation Test using the annotation version GO Ontology database. For the functional classification, the same list of genes was used in a Panther functional classification analysis selecting the ontology Biological Process and the ontology Molecular Function.

Immunohistochemistry

The culture medium was aspirated, cells washed once in PBS, then fixed in 4% PFA in PBS for 15 minutes at room temperature, followed by three PBS washes of 3 min each. Cells were permeabilised and blocked for 1 hour (2% BSA, 0.3% Triton x100 in PBS). Cells were washed in PBS and incubated with primary antibodies overnight at 4°C. Cells were washed in PBS (3x, 15 min) and incubated with secondary antibodies for 2 hrs at room temperature. Cells were washed in PBS (3x, 15 minutes) before imaging in PBS in the wells. Images were taken using a Zeiss Axiovert fluorescence microscope. Working dilutions of the antibodies were as follows: anti-HMOX1, 1:100; anti-mCherry, 1:100; anti-Oct3/4, 1:100; anti-Pax2, 1:200; anti-LHX1, 1:100; anti-

CALB, 1:200; anti-WT1, 1:200; anti-CDH1, 1:300; anti-NPHS1, 1:200; anti-BRACHYURY, 1:100. Details of the used antibodies are listed in the key resources table. Antibody solutions were prepared using PBS containing 1% BSA.

Transporter assays

The transporter assay for organic anion uptake on 20-day 3D renal organoids were performed using the method of (Lawrence, Chang and Davies, 2015). Probenecid was purchased from Sigma-Aldrich, 6-carboxyfluorescein was purchased from Invitrogen (6-CF) and Rhodamine-conjugated peanut agglutinin was purchased from Vector Laboratories. 6-carboxyfluorescein was solubilised in water to make a stock concentration of 1 mM. Probenecid was solubilised in 500 mM NaOH, to make a stock concentration of 250 mM. Reagents for live assays were diluted to their final concentrations in APEL culture medium. The transporter assay for organic cation uptake was performed as follows: 20-day differentiated organoids were incubated overnight with biotin-conjugated LTL (final concentration 20 µg/mL in APEL medium) to label the proximal tubules. After washing, the organoids were incubated for 1 hour at 37°C with streptavidin-conjugated Alexa Fluor 350 (final concentration 10 µg/mL in culture medium). After a further wash, organoids were incubated with 4-(4-(dimehylaminostyryl))-N-methylpyridinium iodide (Asp+) for 30 minutes. For the inhibitor-treated organoids, the OCT2 inhibitor tetrapentyl ammonium chloride (TPA) (final concentration 1 mM) was incubated with the organoids for 10 minutes before addition of the Asp+ (still in the presence of TPA), and incubating for a further 30 minutes. After incubation organoids in both assays were washed in ice cold PBS and transferred to a microscope slide, covered with one drop of ice-cold PBS and imaged immediately.

Verifying HO1-mCherry-hiPSC stress response

Gentamicin was purchased from Sigma-Aldrich (G1397) at a stock concentration of 50mg/ml. Cisplatin was purchased from Tocris (2251) and was diluted in phosphate-buffered saline (PBS) to make a stock concentration

of 100μM. Compounds were diluted in culture medium (E8) at the appropriate concentrations to treat the flat renal organoids. Flat renal organoids were cultured in 24-well plates.

Blind-coded screen

A panel of 7 compounds for the blind-coded validation, selected and supplied by the Gothenburg authors without revealing their identities to the Edinburgh authors, was as follows: Cidofovir, Cisplatin, Dexamethasone, Gentamicin, Ifosfamide, Ketoprofen and Puromycin; all from Sigma-Aldrich. The compounds were divided into 3 groups based on their therapeutic Cmax values (Sjögren *et al.*, 2018) and concentration ranges were designed accordingly: 0.375-24 μM for Dexamethasone and Puromycin, 6-384 μM for Cisplatin, Gentamicin and Ketoprofen, 24-1536 μM for Cidofovir and Ifosfamide. A four-fold dilution series of each blinded compound (lyophilized, obtained from the Gothenburg authors) was prepared and HO1-mCherry-hiPSC-derived renal organoids (flat and 3D) were incubated in these dilutions for either 24h or 72h (Figure 5). A no-treatment control was included for each compound, time-point and organoid type (flat or 3D). 24h flat organoids were cultured in 4 x wells of a 24-well plate; 72h flat organoids in wells of a 96-well plate and 3D organoids on transwell inserts.

QUANTIFICATION AND STATISTICAL ANALYSIS

Fluorescence Measurement

Fluorescence measurements were taken after 24h or 72h. Each live organoid was imaged either 5 times with 4 replicates (flat organoids, 24h), once with 10 replicates (flat organoids, 72h), once with 3 replicates (3D organoids, 24h) or 3 times with 3 replicates (3D organoids, 72h). Organoids were imaged using a Zeiss Axiovert microscope with Axiovision software. All images used for fluorescence intensity analysis were taken with identical exposures and settings. All images were analysed using ImageJ. The total fluorescence intensity of the image was multiplied by the total area with a signal between 600 (lower threshold) and 4096 (higher threshold), where 0 is completely

black and 4096 is completely white. Thus, only signal above a certain threshold is measured in order to discount very dark areas with no cells.

Statistical Analysis

Fluorescence intensity measurements for each concentration of each compound were compared to their respective untreated measurements using Welch's unequal variances t-test (unpaired) with a null hypothesis that there is no significant difference between the experiment and the control. In graphs, a single star indicates a *p* value of the null hypothesis being true of less than 0.05, two stars a *p* value of less than 0.01 and 3 stars a *p* value of less than 0.001. Calculation of the overall performance of the assay (in the Discussion section) was performed by calculating the Wilson Score Interval method (Newcombe, 1998).

Figure S1. Validation of differentiation of wild-type hiPSC-derived renal organoids, Related to Figure 1. (Legend appears on the next page).

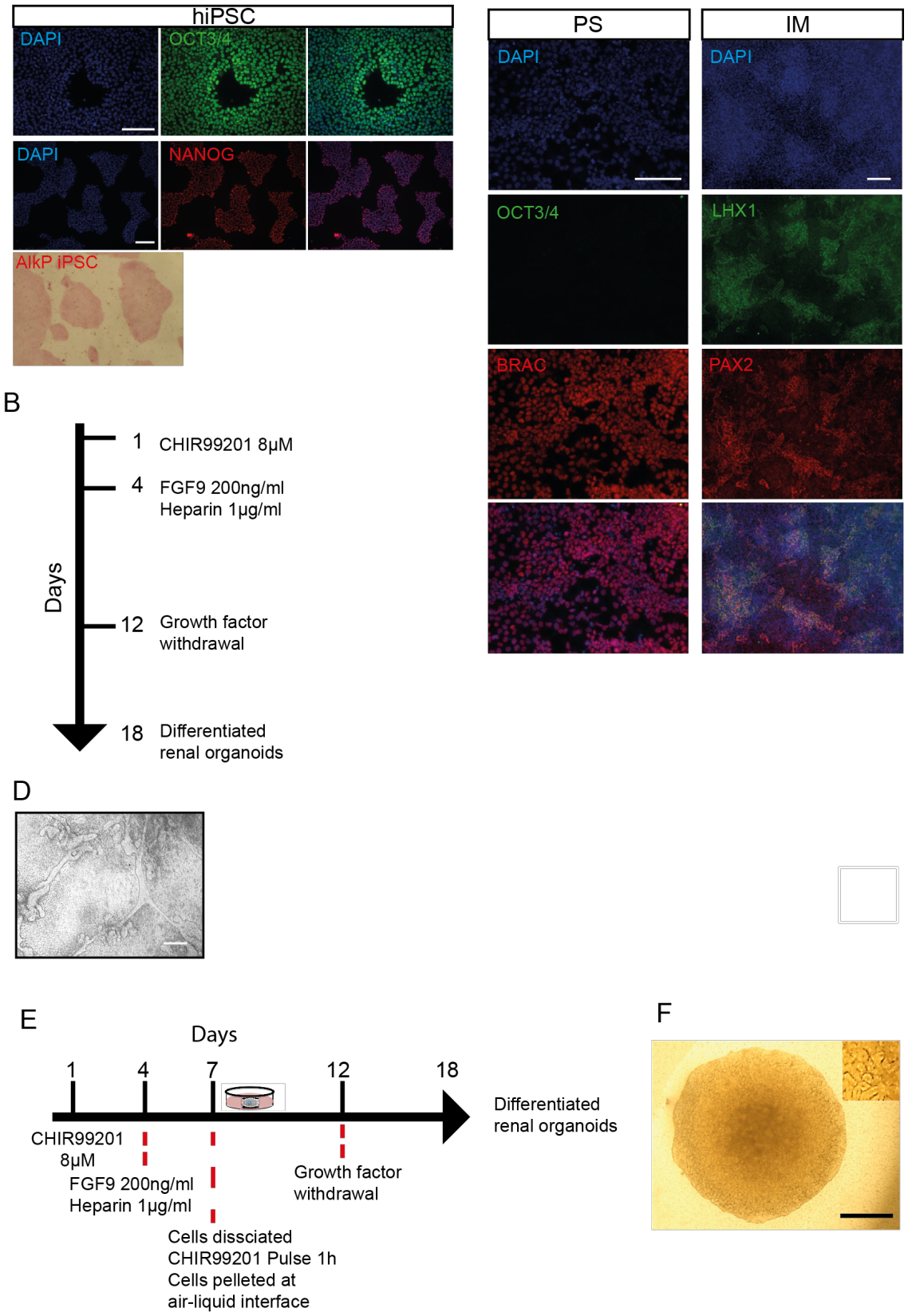

A) Undifferentiated hiPSCs express the markers of pluripotency hOCT3/4 (green, top panels) and hNANOG (red, middle panels) and are positive for the alkaline phosphatase assay (lower panel). B) Differentiation protocol used for induction of flat renal organoids (Takasato et al., 2015). C) hiPSCs lose OCT3/4 expression and express the primitive streak (PS) marker Brachyury (red) after 2 days in culture (left panel PS), and express the markers of intermediate mesoderm (IM) PAX2 (red) and LHX1 (green) (right panel IM) after 9 days. D) Brightfield image of a flat renal organoid. E) Differentiation protocol for induction of 3D renal organoids. F) Brightfield image of renal organoid in a 3D (dome-shaped) format. Scale bars are 100µm (1A-E) or 1mm (1F).

Figure S2. RNA-seq expression analyses for various transporters in wild type, untreated hiPSC-derived flat renal organoids, Related to Figure 1.

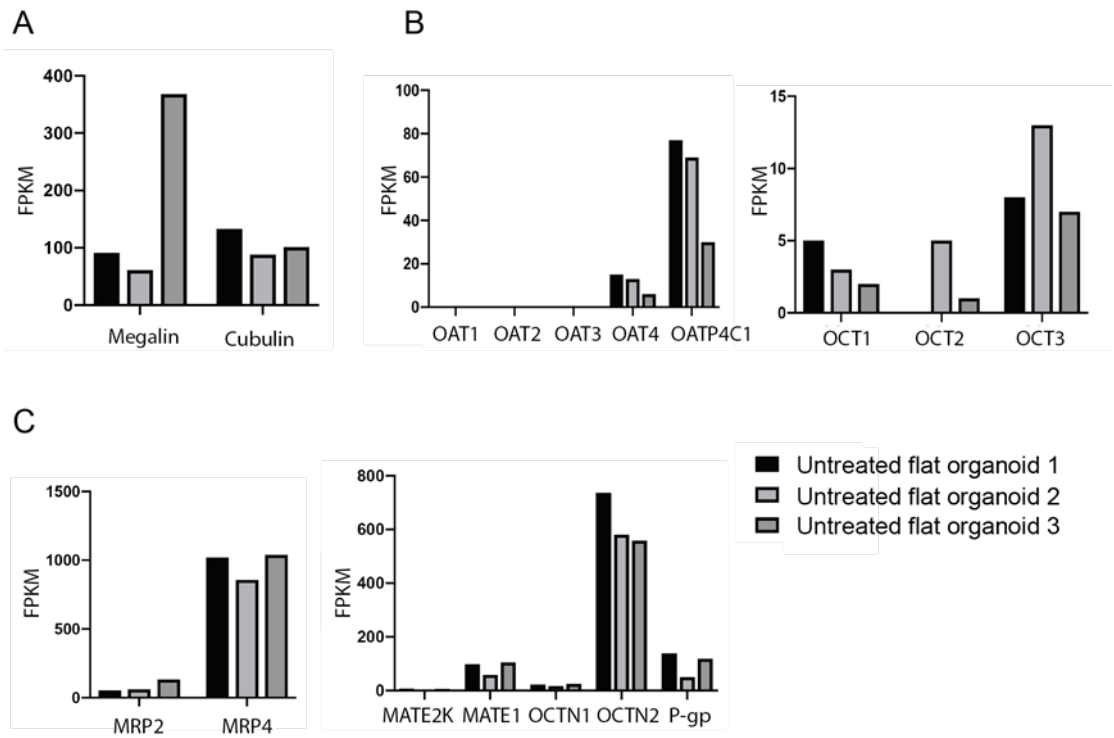

Expression of *Megalin* and *Cubulin* (A), organic anion and cation uptake transporters (B) and efflux transporters (C) in untreated hiPSC-derived flat renal organoids by RNA-seq transcript analyses. FPKM: fragments per kilobase of transcript per Million mapped reads. Transcript analyses for each of the three untreated organoids are shown (Organoids 1-3 in legend).

Figure S3. HMOX1 expression in 3D organoids in response to nephrotoxicants, Related to Figure 2.

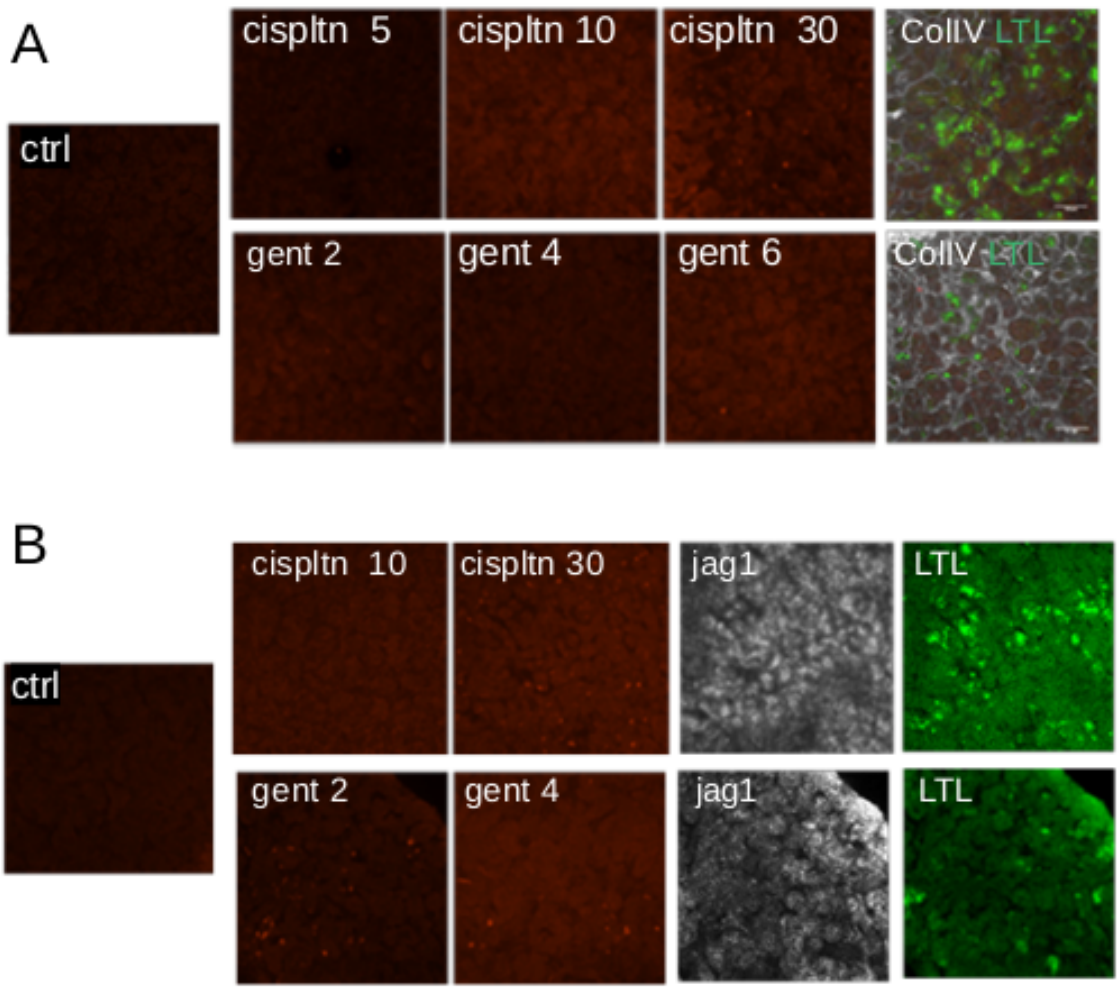

3D organoids are treated with either cisplatin or gentamicin at the concentrations stated in each micrograph (μM for cisplatin, mg/ml for gentamicin): each HMOX expression micrograph was taken at a constant exposure within Fig S3A, and a constant exposure within Fig S3B. Treated samples were also stained for LTL and COL IV (A), or LTL and JAG1 (B). The organoids show increase in HMOX1 expression in response to the toxicant treatment, but ubiquitously, with no apparent concentration of response in proximal tubules or any other component.

3D organoids are treated with either cisplatin or gentamicin at the concentrations stated in each micrograph (μM for cisplatin, mg/ml for gentamicin): each HMOX expression micrograph was taken at a constant exposure within Fig S3A, and a constant exposure within Fig S3B. Treated samples were also stained for LTL and COL IV (A), or LTL and JAG1 (B). The organoids show increase in HMOX1 expression in response to the toxicant treatment, but ubiquitously, with no apparent concentration of response in proximal tubules or any other component. Scale bar (on top right image) 50μm.

Figure S4. Strategy and validation of reporter cassette insertion into hiPSCs, Related to Figure 3.

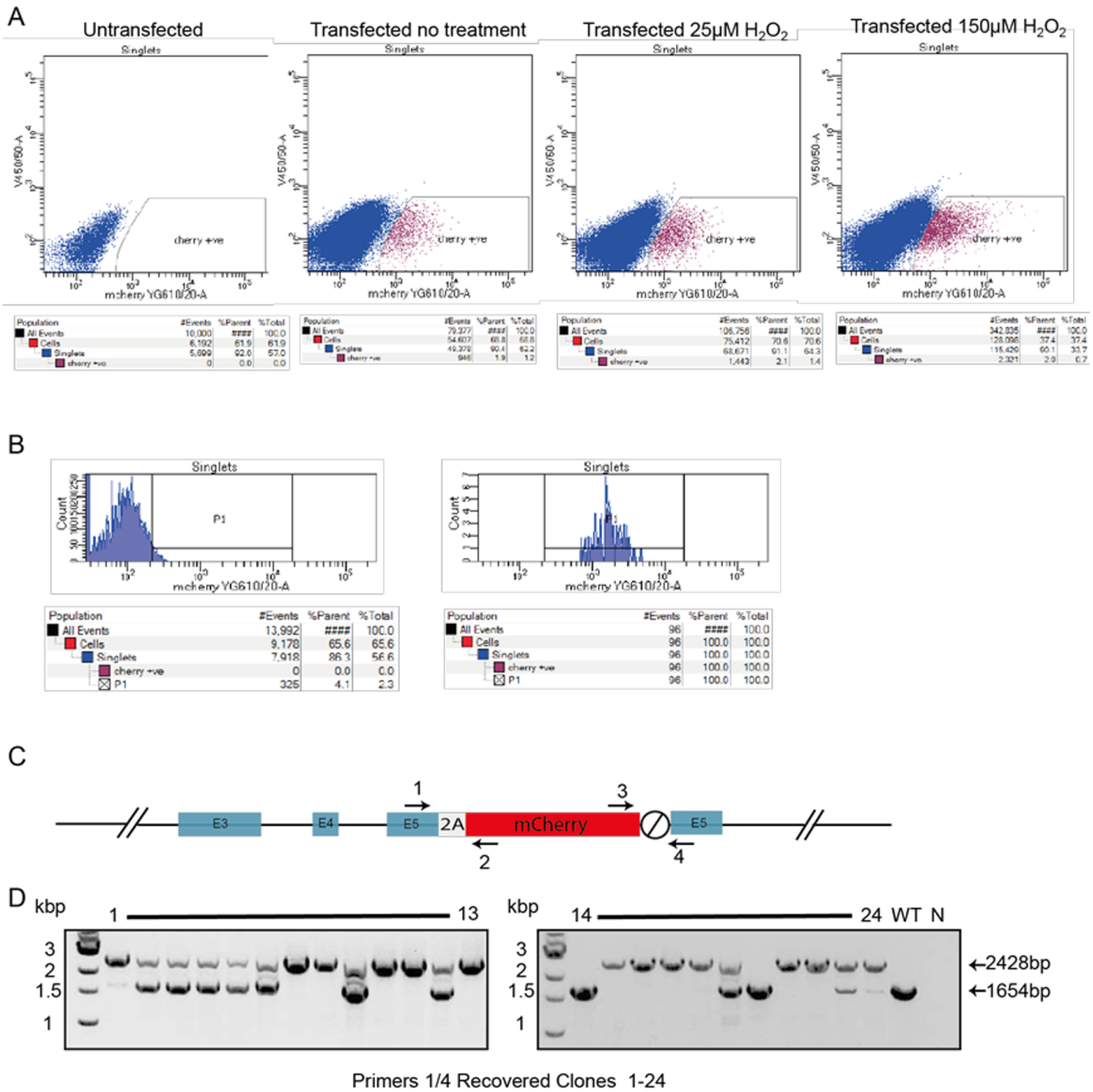

Targeting strategy and clone isolation for *HO1*-mCherry-hiPSC reporter lines. A) Enrichment of targeted cells by fluorescence activated cell sorting (FACS) of either un-transfected (wt) hiPSCs, or CRISPR targeted hiPSCs with 0, 25 or 150μM hydrogen peroxide to induce expression of *HMOX1* through induction of oxidative stress. Basal *HMOX1* expression allowed recovery of cells

containing the 2A-mCherry insertion without hydrogen peroxide treatment. B) Single mCherry-positive cells were sorted into each well of 96-well plates as shown in the right panel to isolate clonal populations. Negative (wild type) cells are shown in the left panel. C) Diagram of the primers designed for verifying cassette insertion into the hiPSC genome. D) PCR products using primer pair 1 and 4 shown in C) - endogenous allele 1654bp, with insertion 2428bp.

Figure S5. *HMOX1* expression in flat and 3D *HO1*-mCherry-hiPSC-derived flat and 3D organoids by qPCR fold-change analysis, Related to Figure 6.

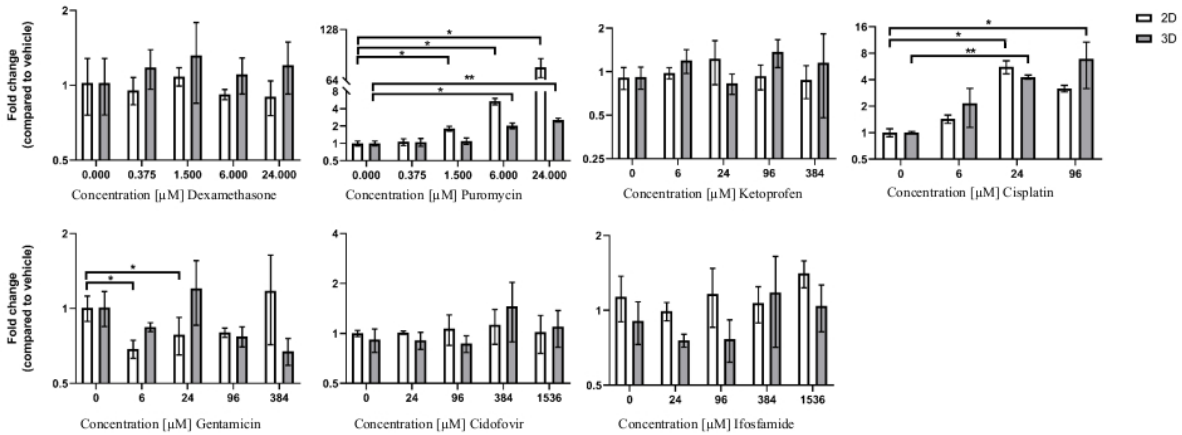

HMOX1 expression fold-change compared to vehicle control in flat (white) and 3D (grey) organoids after 24h treatment with Dexamethasone, Puromycin, Ketoprofen, Cisplatin, Gentamicin, Cidofovir, Ifosfamide, n = 3, ±SD, * < 0.05, ** < 0.01. Cisplatin: no cDNA obtained for highest concentration (384µM), due to massive cell death.

Table S1. Expression of stress-related genes in gentamicin-treated wild type hiPSC-derived flat renal organoids, Related to Figure 2.

Gene Name	Log_2FC	FDR (False Discovery Rate)
LTA	3.873178046	0.000126499
HSPA1B	2.886613617	3.26E-05
JDP2	1.881787141	7.10E-05
HSPA1A	2.663259915	1.75E-05
HSPA6	5.205504565	3.52E-05
ATF3	3.080254651	0.000376849
FOS	3.870520570	0.000598260
JUN	1.372582654	0.022640799
HRK	3.327710653	0.001257237
KIM1	1.669097501	0.031340852
HMOX1	6.552266071	0.000147085

False discovery rate (FDR) 0.05; Log fold-change cut-off 2. The list is not exhaustive and all details can be found in the archived experimental data in the University of Edinburgh database (https://datashare.is.ed.ac.uk/).

Table S2. Analysis of RNA-seq data by GO-term, Related to Figure 2.

GO biological process term	# ref genes in category	GO-term dist 100 top genes	Expected based on chance	Fold enrichment	Significance (p value)	Significance with FDR adjustment
detoxification of inorganic compound (GO:0061687)	15	9	0.08	> 100	2.08E-15	3.27E-11
detoxification of copper ion (GO:0010273)	14	8	0.07	> 100	1.08E-13	4.25E-10
stress response to copper ion (GO:1990169)	14	8	0.07	> 100	1.08E-13	3.40E-10
stress response to metal ion (GO:0097501)	16	9	0.08	> 100	3.23E-15	2.54E-11
cellular response to zinc ion (GO:0071294)	22	8	0.11	70.57	1.91E-12	3.01E-09
negative regulation of inclusion body assembly (GO:0090084)	11	4	0.06	70.57	8.50E-07	3.43E-04
cellular response to copper ion (GO:0071280)	26	8	0.13	59.71	5.83E-12	7.65E-09
cellular zinc ion homeostasis (GO:0006882)	31	9	0.16	56.34	4.06E-13	1.06E-09
zinc ion homeostasis (GO:0055069)	34	9	0.18	51.37	8.26E-13	1.63E-09
cellular response to cadmium ion (GO:0071276)	36	9	0.19	48.52	1.29E-12	2.25E-09
PERK-mediated unfolded protein response (GO:0036499)	12	3	0.06	48.52	5.69E-05	1.38E-02
regulation of inclusion body assembly (GO:0090083)	17	4	0.09	45.66	3.64E-06	1.22E-03
response to copper ion (GO:0046688)	41	8	0.21	37.87	1.36E-10	1.43E-07
protein refolding (GO:0042026)	21	4	0.11	36.97	7.57E-06	2.34E-03
chaperone cofactor-dependent protein refolding (GO:0051085)	28	5	0.14	34.66	6.78E-07	2.81E-04
response to zinc ion (GO:0010043)	54	9	0.28	32.35	3.19E-11	3.86E-08

response to cadmium ion (GO:0046686)	62	10	0.32	31.3	3.26E-12	4.66E-09
'de novo' posttranslational protein folding (GO:0051084)	33	5	0.17	29.4	1.40E-06	5.26E-04
positive regulation of erythrocyte differentiation (GO:0045648)	28	4	0.14	27.72	2.09E-05	6.10E-03
chaperone-mediated protein folding (GO:0061077)	56	8	0.29	27.72	1.25E-09	1.10E-06
'de novo' protein folding (GO:0006458)	37	5	0.19	26.23	2.34E-06	8.01E-04
regulation of cellular response to heat (GO:1900034)	45	6	0.23	25.88	2.33E-07	1.11E-04
cellular transition metal ion homeostasis (GO:0046916)	105	13	0.54	24.03	3.37E-14	1.77E-10
transition metal ion homeostasis (GO:0055076)	132	13	0.68	19.11	5.01E-13	1.13E-09
detoxification (GO:0098754)	110	10	0.57	17.64	5.77E-10	5.67E-07
regulation of erythrocyte differentiation (GO:0045646)	44	4	0.23	17.64	1.06E-04	2.43E-02
negative regulation of fat cell differentiation (GO:0045599)	45	4	0.23	17.25	1.15E-04	2.59E-02
positive regulation of blood vessel endothelial cell migration (GO:0043536)	54	4	0.28	14.38	2.23E-04	4.74E-02
response to unfolded protein (GO:0006986)	154	10	0.79	12.6	1.21E-08	9.07E-06
positive regulation of ubiquitin-dependent protein catabolic process (GO:2000060)	94	6	0.48	12.39	1.26E-05	3.74E-03
positive regulation of proteasomal ubiquitin-dependent protein catabolic process (GO:0032436)	81	5	0.42	11.98	8.02E-05	1.91E-02
cellular response to metal ion (GO:0071248)	185	11	0.95	11.54	5.17E-09	4.28E-06
cellular response to unfolded protein (GO:0034620)	118	7	0.61	11.51	3.66E-06	1.20E-03
response to heat (GO:0009408)	104	6	0.54	11.2	2.17E-05	6.11E-03
response to topologically incorrect protein (GO:0035966)	174	10	0.9	11.15	3.63E-08	2.28E-05
negative regulation of growth (GO:0045926)	256	14	1.32	10.61	1.03E-10	1.16E-07
transition metal ion transport (GO:0000041)	110	6	0.57	10.59	2.94E-05	7.83E-03
cellular response to inorganic substance (GO:0071241)	208	11	1.07	10.26	1.64E-08	1.12E-05
cellular response to topologically incorrect protein (GO:0035967)	136	7	0.7	9.99	8.90E-06	2.69E-03
positive regulation of proteolysis involved in cellular protein catabolic process (GO:1903052)	117	6	0.6	9.95	4.09E-05	1.04E-02
positive regulation of proteasomal protein catabolic process (GO:1901800)	102	5	0.53	9.51	2.25E-04	4.72E-02
positive regulation of cellular protein catabolic process (GO:1903364)	137	6	0.71	8.5	9.46E-05	2.19E-02
protein folding (GO:0006457)	208	9	1.07	8.4	1.75E-06	6.41E-04
regulation of ubiquitin-dependent protein catabolic process (GO:2000058)	147	6	0.76	7.92	1.37E-04	3.00E-02
response to metal ion (GO:0010038)	358	13	1.84	7.05	5.52E-08	3.22E-05
response to toxic substance (GO:0009636)	482	17	2.48	6.84	6.16E-10	5.71E-07
cellular metal ion homeostasis (GO:0006875)	532	16	2.74	5.84	1.84E-08	1.21E-05
response to inorganic substance (GO:0010035)	515	14	2.65	5.28	5.11E-07	2.17E-04
cellular cation homeostasis (GO:0030003)	591	16	3.05	5.25	7.58E-08	4.26E-05
cellular divalent inorganic cation homeostasis (GO:0072503)	444	12	2.29	5.25	3.77E-06	1.21E-03
metal ion homeostasis (GO:0055065)	601	16	3.1	5.17	9.48E-08	4.97E-05
cellular ion homeostasis (GO:0006873)	604	16	3.11	5.14	1.01E-07	5.14E-05
divalent inorganic cation homeostasis (GO:0072507)	466	12	2.4	5	6.08E-06	1.92E-03
ion homeostasis (GO:0050801)	743	19	3.83	4.96	9.46E-09	7.44E-06
regulation of growth (GO:0040008)	679	17	3.5	4.86	8.49E-08	4.61E-05

cellular chemical homeostasis (GO:0055082)	693	17	3.57	4.76	1.13E-07	5.55E-05
cation homeostasis (GO:0055080)	664	16	3.42	4.68	3.52E-07	1.58E-04
inorganic ion homeostasis (GO:0098771)	676	16	3.48	4.59	4.45E-07	1.94E-04
cellular homeostasis (GO:0019725)	842	18	4.34	4.15	3.36E-07	1.56E-04
regulation of cellular response to stress (GO:0080135)	654	12	3.37	3.56	1.53E-04	3.31E-02
chemical homeostasis (GO:0048878)	1050	19	5.41	3.51	1.79E-06	6.40E-04
negative regulation of cell death (GO:0060548)	999	16	5.15	3.11	5.61E-05	1.38E-02
homeostatic process (GO:0042592)	1558	24	8.03	2.99	1.05E-06	4.15E-04
regulation of apoptotic process (GO:0042981)	1510	21	7.78	2.7	2.66E-05	7.34E-03
regulation of programmed cell death (GO:0043067)	1523	21	7.85	2.68	3.01E-05	7.91E-03
regulation of cell death (GO:0010941)	1643	22	8.47	2.6	2.92E-05	7.93E-03
cellular response to stress (GO:0033554)	1582	21	8.15	2.58	5.22E-05	1.30E-02
cellular response to chemical stimulus (GO:0070887)	2674	33	13.78	2.4	1.20E-06	4.59E-04
response to stress (GO:0006950)	3290	40	16.95	2.36	5.30E-08	3.21E-05
response to organic substance (GO:0010033)	2787	31	14.36	2.16	2.13E-05	6.09E-03
negative regulation of biological process (GO:0048519)	5021	53	25.87	2.05	1.31E-08	9.35E-06
response to chemical (GO:0042221)	4172	43	21.5	2	1.93E-06	6.76E-04
regulation of biological quality (GO:0065008)	3814	36	19.65	1.83	1.30E-04	2.88E-02
negative regulation of cellular process (GO:0048523)	4482	42	23.09	1.82	3.82E-05	9.87E-03
response to stimulus (GO:0050896)	7985	61	41.14	1.48	8.95E-05	2.10E-02

Column 1: PANTHER GO-term category. Column 2: Number of reference genes in each category. Column 3: GO term distribution of 100 most up-regulated genes in response to gentamicin-treated flat renal organoids. Column 4: Number of genes expected based on chance. Column 5: Fold-enrichment of the up-regulated genes in each GO term category. Column 6: Significance of gene enrichment compared to expected (*p* value). Column 7: Significance after applying False Discovery Rate (FDR) adjustment.

Table S3. - Significant fold-changes of *HMOX1* biomarker gene expression in flat and 3D *in vitro* kidney organoids after 24h drug treatment, Related to Figure 6 and Figure S5.

Drug	Organoid Type	Concentration (low ➔ high)			
Dexamethasone	Flat	ns	ns	ns	ns
	3D	ns	ns	ns	ns
Ketoprofen	Flat	ns	ns	ns	ns
	3D	ns	ns	ns	ns
Puromycin	Flat	ns	*	*	**
	3D	ns	ns	*	**
Cisplatin	Flat	ns	*	*	N/A
	3D	ns	**	ns	N/A
Gentamicin	Flat	*	*	ns	ns
	3D	ns	ns	ns	ns
Cidofovir	Flat	ns	ns	ns	ns
	3D	ns	ns	ns	ns
Ifosfamide	Flat	ns	ns	ns	ns
	3D	ns	ns	ns	ns

Significance determined by repeated measure one-way ANOVA on $2^{-\Delta\Delta CT}$ values compared to the vehicle control, ns: non-significant, * < 0.05, ** < 0.01, increase indicated in blue, decrease indicated in red.

Table S4. Summary of gRNA and primer sequences for RT-PCR, and TaqMan assay numbers, Related to Figure 3A.

Description/Name	**Sequence**
HMOX1 gRNA1 for CRISPR targeting	CACCGGCTTTATGCCATGTGAATGC
HMOX1 gRNA2 for CRISPR targeting	CACCGGCCAGCATGCCTGCATTCACA
Human *OAT1 (SLC22A6)* forward primer	AGTCCTTGTACATGGTGGGG
Human *OAT1 (SLC22A6*) reverse primer	CATGCAGTTGAGGGAGATGC
Human *OCT2 (SLC22A2)* forward primer	CCGTAAGCTCTGCCTCCTAA
Human *OCT2 (SLC22A2)* reverse primer	TGTTCTCCGATATCTCCGCC
Human *Megalin (LRP2)* forward primer	AACGAGACGCACAGTAGTTCA
Human *Megalin (LRP2)* reverse primer	GTGAAGCAGCCCAATCGATG
Human *Cubulin (CUBN)* forward primer	TCGTCTCCTCAGGAAACAGC
Human *Cubulin (CUBN)* reverse primer	TGGAGGTTGCGCTTGAATGA
HMOX1 Targeting verification primer 1	AGGGATGGGACTGAACTTGA
β-actin (ACTB) forward primer	CTGGGACGACATGGAGAAAA
β-actin (ACTB) reverse primer	AAGGAAGGCTGGAAGAGTGC
HMOX1 Targeting verification primer 2	ACCTTGAAGCGCATGAACTC
HMOX1 Targeting verification primer 3	ACAACGAGGACTACACCATC
HMOX1 Targeting verification primer 4	AATATTCGCCCACCAGCTAC
Hprt1 TaqMan Reference ID	Mm00446968_m1
HMOX1 (HO1) Taqman Reference ID	Hs01110250_m1

Table S5. The 100 most up-regulated genes classified by overlap in various gene categories that they belong to using GO classification, Related to Figure 2.

Names	Total	Elements
Binding MF, Biolog Regul BP, Catal Act MF, Cellul Proc BP, Metab Proc BP, Resp to Stim BP	2	TRIB3, HMOX1
Binding MF, Catal Act MF, Cellul Proc BP, Metab Proc BP, Resp to Stim BP	3	HSPA6, HSPA1B, HSPA1A
Binding MF, Catal Act MF, Cellul Proc BP, Metab Proc BP	3	ASNS, FKBP4, TSPYL2
Binding MF, Cellul Proc BP, Metab Proc BP, Resp to Stim BP	2	INHBE, MSTN
Binding MF, Biolog Regul BP, Cellul Proc BP, Metab Proc BP	1	HIST1H2AG
Binding MF, Biolog Regul BP, Cellul Proc BP, Resp to Stim BP	2	LRG1, EGF
Catal Act MF, Cellul Proc BP, Metab Proc BP, Resp to Stim BP	1	PPP1R15A
Biol Regul BP, Catal Act MF, Cellul Proc BP, Metab Proc BP	3	DIO3, GCLM, CES1
Binding MF, Cellul Proc BP, Metab Proc BP	6	SFBQ, PSPC1, GCM1, DNAJB1, ATF5, JDP2
Binding MF, Cellul Proc BP, Resp to Stim BP	1	LTA
Binding MF, Biol Regul BP, Cellul Proc BP	2	FTH1, FTL
Binding MF, Biolog Regul BP, Metab Proc BP	1	ID2
Catal Act MF, Cellul Proc BP, Metab Proc BP	6	UAP1L1, WARS, BAAT, HTRA3, B3GALNT2, ABCC3
Biolog Regul BP, Cellul Proc BP, Resp to Stim BP	3	CASS4, SLC30A2, GABRR2
Binding MF, Cellul Proc BP	3	CHORDC1, TUBB3, AVIL
Binding MF, Metab Proc BP	1	BRPF3
Catal Act MF, Cellul Proc BP	2	ME1, NEURL3
Catal Act MF, Metab Proc BP	2	CHKA, ASPRV1
Cellul Proc BP, Metab Proc BP	2	SLC1A4, ZNF425

Binding MF	4	ZFAND2A, CNN1, SQSTM1, MRPL18
Cellul Proc BP	8	SLC38A10, SLC7A11, GATA2, MC1R, RRAD, SCFD2, MYH15, RASL11A
Metab Proc BP	1	ANXA1

1

2